George S. Karagiannis, Natasha Musrap, Punit Saraon, Ann Treacy, David F. Schaeffer, Richard Kirsch, Robert H. Riddell and Eleftherios P. Diamandis*

Bone morphogenetic protein antagonist gremlin-1 regulates colon cancer progression

Abstract: Bone morphogenetic proteins (BMP) are phylogenetically conserved signaling molecules of the transforming growth factor-beta (TGF-beta) superfamily of proteins, involved in developmental and (patho)physiological processes, including cancer. BMP signaling has been regarded as tumor-suppressive in colorectal cancer (CRC) by reducing cancer cell proliferation and invasion, and by impairing epithelial-to-mesenchymal transition (EMT). Here, we mined existing proteomic repositories to explore the expression of BMPs in CRC. We found that the BMP antagonist gremlin-1 (GREM1) is secreted from heterotypic tumor-host cell interactions. We then sought to investigate whether GREM1 is contextually and mechanistically associated with EMT in CRC. Using immunohistochemistry, we showed that GREM1-expressing stromal cells harbor prominent features of myofibroblasts (i.e., cancer-associated fibroblasts), such as expression of α-smooth muscle actin and laminin-beta-1, and were in contextual proximity to invasion fronts with loss of the tight junction protein occludin and parallel nuclear accumulation of β-catenin, two prominent EMT hallmarks. Furthermore, *in vitro* assays demonstrated that GREM1-dependent suppression of BMP signaling results in EMT induction, characterized by cadherin switching (loss of E-cadherin-upregulation of N-cadherin) and overexpression of Snail. Collectively, our data support that GREM1 promotes the loss of cancer cell differentiation at the cancer invasion front, a mechanism that may facilitate tumor progression.

Keywords: angiogenesis; bone morphogenetic protein; cancer-associated fibroblasts; colorectal cancer; epithelial-to-mesenchymal transition; gremlin-1; stroma; tumor microenvironment.

DOI 10.1515/hsz-2014-0221
Received June 26, 2014; accepted August 1, 2014; previously published online August 6, 2014

***Corresponding author: Eleftherios P. Diamandis,** Department of Laboratory Medicine and Pathobiology, University of Toronto, Toronto, Ontario, Canada; Department of Pathology and Laboratory Medicine, Mount Sinai Hospital, Joseph and Wolf Lebovic Ctr., 60 Murray St., Toronto M5T 3L9, Ontario, Canada; and Department of Clinical Biochemistry, University Health Network, Toronto, Ontario, Canada, e-mail: ediamandis@mtsinai.on.ca
George S. Karagiannis, Natasha Musrap and Punit Saraon: Department of Laboratory Medicine and Pathobiology, University of Toronto, Toronto, Ontario, Canada; and Department of Pathology and Laboratory Medicine, Mount Sinai Hospital, Joseph and Wolf Lebovic Ctr., 60 Murray St., Toronto M5T 3L9, Ontario, Canada
Ann Treacy: MC Pathology, the Laboratory, Charlemont Clinic, Charlemont Mall, Dublin 2, Ireland
David F. Schaeffer: Department of Pathology and Laboratory Medicine, University of British Columbia, Vancouver V5Z 1M9, British Columbia, Canada
Richard Kirsch and Robert H. Riddell: Department of Pathology and Laboratory Medicine, Mount Sinai Hospital, Joseph and Wolf Lebovic Ctr., 60 Murray St., Toronto M5T 3L9, Ontario, Canada

Introduction

Bone morphogenetic proteins (BMPs) are a group of phylogenetically conserved signaling molecules, which belong to the transforming growth factor-β (TGF-β) superfamily of proteins, and were initially shown to induce endochondral bone formation (Chen et al., 2004). During embryonic life, BMPs are responsible for neurogenesis, hematopoiesis, reduction of limb bud outgrowth and formation of osteoblast and chondrocyte precursors (Kishigami and Mishina, 2005). After birth, BMPs are involved in skeletal homeostasis, mainly by promoting the maintenance of bone mass (Miyazono et al., 2005). BMP signaling is mediated through type I and type II serine/threonine kinase receptors. Upon ligand binding, the type II receptor forms a heterodimer with type I receptor and the constitutive kinase of the type II receptor activates the type I receptor. Such activation may initiate signal transduction through phosphorylation of downstream factors [i.e., mothers against decapentaplegic (Smads)], which further causes their translocation into the nucleus, where they inhibit or activate transcription of target genes (Miyazono et al., 2005).

In the normal colon, BMPs are primarily produced by epithelial cells to sustain epithelial phenotype and polarity at the level of the colonic crypt (Hardwick et al.,

2004). However, this pathway has been considered as a major barrier to the development of intestinal cancer, and various mechanisms, including genetic, epigenetic and/or extracellular ones, seem to be conscientious for its impairment (Hardwick et al., 2008). The most important hallmark acquired from BMP-suppression seems to be the disruption of the epithelial phenotype, possibly through the deployment of epithelial-to-mesenchymal transition (EMT) (Hardwick et al., 2004; Karagiannis et al., 2012b), an event that is quite critical for the effective propagation of the metastatic cascade (Kalluri, 2009; Kalluri and Weinberg, 2009; Hanahan and Weinberg, 2011). Despite an inhibitory effect of BMPs on the Wnt pathway that has been previously documented (He et al., 2004; Bertrand et al., 2012), the exact contribution of BMPs and their antagonists in CRC progression, and especially EMT, are only poorly understood.

Currently, high-throughput proteomics coupled to mass spectrometry and bioinformatics play key roles in the identification, quantification and characterization of proteins in complex biological samples (Kulasingam and Diamandis, 2008; Karagiannis et al., 2010), and their emergence has benefited cancer research (i.e., oncoproteomics) with a plethora of opportunities for rationalized diagnosis and management (Jain, 2008; Karagiannis et al., 2010). Using proteomics, we previously defined protein expression signatures with potential involvement in tumor-host cell interactions (Karagiannis et al., 2012a), and subsequently targeted the BMP pathway as potential mediator of cancer progression (Karagiannis et al., 2013; Karagiannis et al., 2014c). Here, we perform meta-mining of these proteomic repositories to explore the expression levels of BMPs and their regulators and show that the BMP antagonist gremlin-1 (GREM1) is strongly expressed in CRC desmoplastic invasion fronts. Further, we provide preliminary evidence that GREM1 is not only contextually correlated with cancer cells undergoing EMT in tissues with invasive colorectal carcinomas, but that it also mediates EMT by specifically disrupting the BMP7-dependent promotion of epithelial phenotype *in vitro*.

Results

Proteomic and *in silico* investigations of the BMP pathway in colorectal cancer

Using a well-established mass spectrometry-based method for proteomic analysis of cancer cell supernatants (i.e., 'secretome analysis') (Kulasingam and Diamandis, 2008), we had previously delineated secretome profiles from 13 CRC cell lines (Karagiannis et al., 2014b). We retrieved these data, to examine *in vitro* secretion of BMP2, BMP4 and BMP7 in CRC. BMP2 was absent in all 13 CRC secretomes, BMP4 was identified in all but the RKO secretome and BMP7 was identified in five out of the 13 CRC secretomes, namely the SW1116, SW480, SW620, LS174T and Colo205 ones (Figure 1A). In each case, the mean spectral counts of both BMP4 and BMP7 were higher in the SW1116 cell line, the earliest (Duke's Stage A) stage among the 13 cell lines (Figure 1A). Notably, BMP4 and BMP7 secretion displayed a significant reduction ($p<0.025$; Holms-corrected, Jonckheere-Terpstra test) across the increasing Duke's-based staging of the CRC cell lines (Figure 1B), and this occurred in a replication error (RER) status-independent ($p>0.025$, Holms-corrected Mann-Whitney *U*-test) fashion (Figure 1C). Further, we investigated BMP2, BMP4 and BMP7 gene-expression profiles in a cDNA array consisting of 24 CRC patients matched with normal colonic mucosal tissue adjacent to the tumor (Figure S3A–C). Consistently, BMP2 showed a significant ($p<0.007$; Holms-corrected Wilcoxon test) ~4.5-fold downregulation in cancer compared to normal tissues, while BMP4 and BMP7 were significantly ($p<0.007$; Holms-corrected Wilcoxon test) upregulated (~1.4-fold and ~12-fold, respectively) (Figure 1D). We verified gene-expression of the BMP receptors type IA (BMPR1A), IB (BMPR1B) and II (BMPR2) in this patient array, but none of these receptors showed differential expression (Figure 1D; Figure S3D–F).

Given that BMP pathway suppression is strongly documented in sporadic CRC (Kodach et al., 2008), we considered that the aberrant secretion of BMPs by colon cancer cells both *in vitro* and in patient tissues was paradoxical. Thus, we initially sought to verify *in silico* that progression of CRC is characterized by significant overexpression of BMPs and further examined the translational impact of these expressional perturbations in advanced CRC. First, we performed gene-expression meta-analysis (Genevestigator) and found ~3.1-fold increase in the expression of both BMP4 and BMP7, and ~2.2-fold decrease in the expression of BMP2 in colon adenocarcinoma/carcinoma compared to control tissues (Figure 1D). Representative heatmaps from studies showing discriminatory differences in BMP2, BMP4 and BMP7 gene-expression between colon cancer and healthy control tissues are shown (Figure S4). Second, we incorporated survival data from two large datasets totaling 326 (Loboda et al., 2011) and 232 (Smith et al., 2009) CRC patients, respectively, to perform gene-expression-based survival analysis (Goswami and Nakshatri, 2013). This meta-analysis demonstrated that the increased expression of BMP2, BMP4 and BMP7 is each

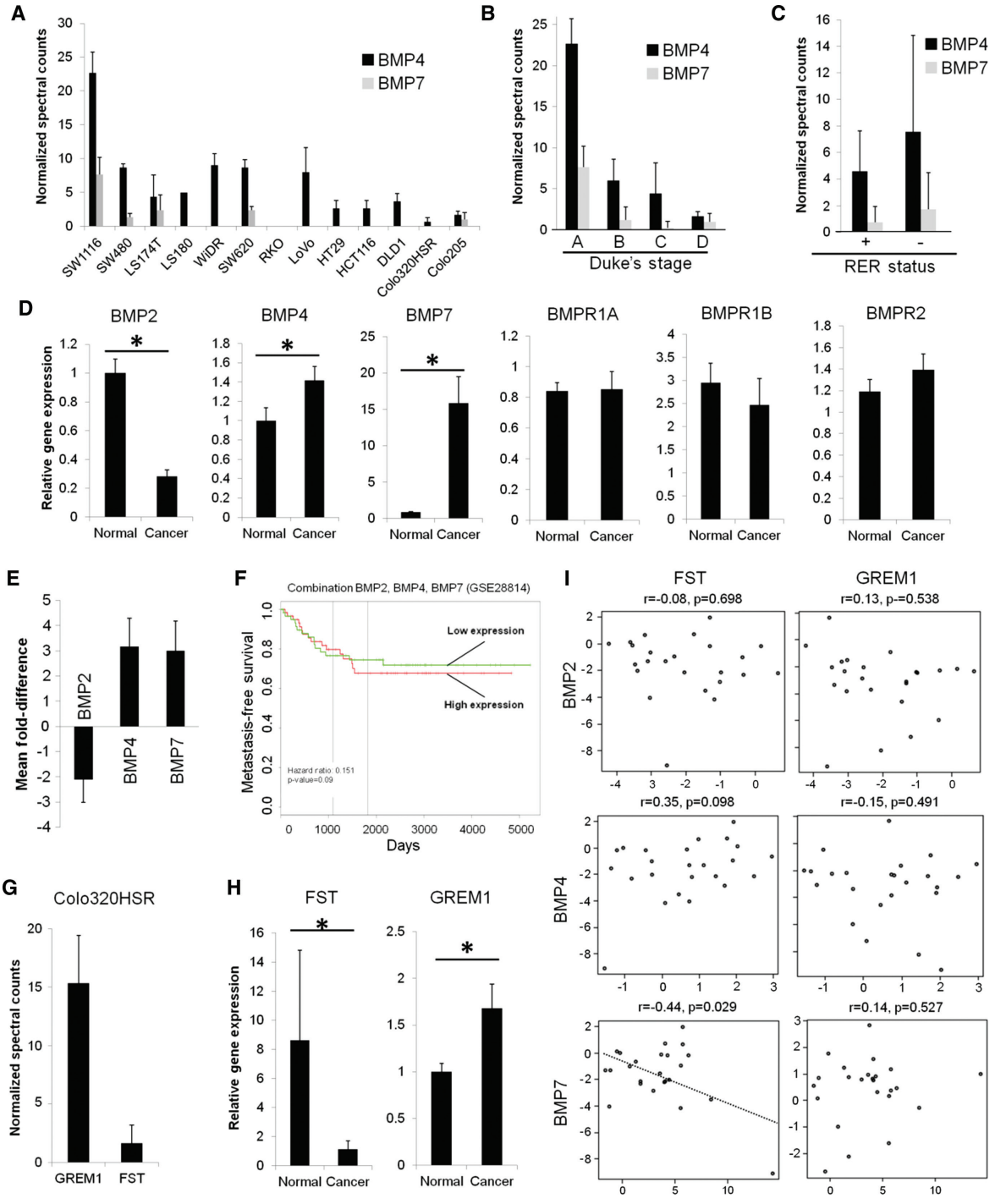

Figure 1 *In vitro* proteomic and *in silico* investigations of BMPs in colorectal cancer.
(A) Mean normalized spectral counts of BMP4 and BMP7 in 13 cell lines. (B) Mean normalized spectral counts of BMP4 and BMP7 in various stages (Duke's system) of CRC. Analysis performed by Jonckheere-Terpstra test. (C) Mean normalized spectral counts of BMP4 and BMP7 by mismatch repair (RER+ and RER-) status. Analysis performed by Mann-Whitney *U*-test. (D) Relative gene-expression levels of BMP2, BMP4 and BMP7, as well as BMPR1A, BMPR1B and BMPR2 between cancer lesions and adjacent healthy areas of CRC patients (cDNA array). Asterisks denote statistical significance, $p<0.007$, Wilcoxon test. (E) Mean fold difference of BMP2, BMP4 and BMP7 across all available microarray experiments of the Genevestigator knowledgebase. (F) Kaplan-Meier metastasis-free survival of the Loboda cohort (Loboda et al., 2011), stratified according to the median of the combined BMP2, BMP4 and BMP7 expression scores. (G) Mean normalized spectral counts of GREM1 and FST in the Colo320HSR cell line. (H) Relative gene-expression levels of FST and GREM1 between cancer lesions and adjacent healthy areas of CRC patients (cDNA array). Asterisks denote statistical significance, $p<0.007$, Wilcoxon test. (I) Scatter plots demonstrating correlation between gene-expression levels of FST or GREM1 and each one of the three major BMPs (BMP2, BMP4 and BMP7) in CRC patients (cDNA array). Statistical significance is shown with $p<0.05$, Spearman's ranked correlation coefficient.

independently associated with worse overall survival in colon cancer, and additionally, their increased expression is mildly associated with worse metastasis-free survival in colon cancer, when all three BMPs are combined in one analysis (Figure 1E, $p<0.1$). Given the above, the claim about tumor-suppressive properties of BMP signaling in CRC seems to be paradoxical at first sight, however, all these observations are in concordance with current literature (Bendtsen et al., 2004; Sääf et al., 2007; Hardwick et al., 2008; Kodach et al., 2008; Slattery et al., 2011a,b).

In an attempt to explain this deviation, we reasoned that despite the significant increase in the expression of the first messengers (i.e., BMPs), the BMP pathway is most probably disrupted via mechanisms exclusive of BMP4/7 downregulation at the diseased tissue level. As most signaling pathways in mammalian cells also target their own antagonists/inhibitors for transcription (negative feedback loop), we first examined the possibility that BMP4/7-expressing CRC cell lines also expressed BMP antagonists. Using the 13 CRC secretome datasets, we examined the expression of two highly selective BMP antagonists, known to bind to and dimerize with BMPs with strong affinity [i.e., gremlin-1 (GREM1) and noggin (NOG)], and one less selective BMP antagonist that binds to BMPs with less affinity [i.e., follistatin (FST)] (Gazzerro and Canalis, 2006; Beites et al., 2009). With the exception of the Colo320HSR cell line, which secreted small amounts of GREM1 and FST, none of the remaining CRC cell lines expressed detectable amounts of any of the BMP antagonists at the proteome level (Figure 1G). We then investigated the expression of GREM1 and FST in the 24-patient cDNA array (Figure S3G, H), and found that FST was significantly ($p<0.007$; Holms-corrected Wilcoxon test) downregulated by ~8-fold, while GREM1 was significantly ($p<0.05$; Holms-corrected Wilcoxon test) upregulated by ~2-fold in neoplastic compared to normal colonic tissue (Figure 1H). Despite the differences in GREM1/FST expression levels between cancerous and normal colon, when we assessed all possible correlations between BMP2/4/7 and GREM1/FST expression in a pair-wise fashion (Figure 1I), we only came across a loose inverse correlation between BMP7 and FST ($p<0.05$, r=-0.44; Spearman's ranked correlation), whereas no significant associations between GREM1 and BMP expression were found.

The BMP antagonist Gremlin-1 is produced by CAFs in desmoplastic invasion fronts

Overall these observations contradict the speculation that GREM1 may act on an autocrine feedback loop to suppress BMP signaling in CRC. On this basis, along with supportive literature evidence (Sneddon et al., 2006; Sneddon, 2009; Karagiannis et al., 2012b, 2013), our next speculation was that GREM1 acts in a paracrine, instead of autocrine, fashion to suppress BMP signaling in CRC and more precisely is expressed/secreted by the desmoplastic microenvironment. In our previous study (Karagiannis et al., 2012a), we had generated *in vitro* cocultures of SW480/SW620 colon cancer cells with the 18Co normal colonic fibroblasts. By performing high-throughput secretome analysis, we had proposed a secreted 152-protein signature coined with the term 'desmoplastic protein dataset' (DPD). By confirming the presence of GREM1 in this signature, we observed that this BMP antagonist was entirely absent from monocultures (Figure 2A). Normalized quantitative values of additional BMP suppressors and antagonists (i.e., FST, FSTL3 and HTRA3), are also indicated in Figure 2A.

For verification, we reproduced these mono- and cocultures (Karagiannis et al., 2012a) and measured GREM1 levels with an immunoassay. GREM1 was secreted by SW480/18Co (SW480Co) and SW620/18Co (SW620Co) cocultures (~15 ng/ml), while only small levels were observed in the control monocultures (SW480, SW620 and 18Co) (Figure 2B). Moreover, when we stimulated 18Co normal colonic fibroblasts with 2-day supernatants derived from either SW480 or SW620 cell lines, we observed a ~4-fold increase in GREM1 gene-expression levels in both cases, suggesting that colonic fibroblasts may elicit increased GREM1 expression in response to paracrine signals (Figure 2C). As negative control, the stimulation of SW480 and SW620 colon cancer cells with 2-day supernatant derived from 18Co cells resulted in non-significant increase of GREM1 (Figure 2C). A similar pattern was observed for two additional BMP suppressors/inhibitors, FST and HTRA3 (Figure 2C). Furthermore, when we mined the literature for supportive data, we found one study (Navab et al., 2011), in which the authors had compared transcriptome profiles of cell lines derived from either CAFs or their normal fibroblastic counterparts (NFs) from patients with non-small lung cell carcinoma (NSCLC). By investigating gene-expression levels of GREM1 in these data, we found that GREM1 was ~6-fold upregulated in CAFs compared to NFs (Figure 2C).

We then retrieved a patient cohort of 30 invasive CRC cases (Karagiannis et al., 2014a,c), from which we selected 42 areas, either encompassing healthy/normal (n=21) or pathologic/desmoplastic (n=21) stromata (Figure 2D). When we compared GREM1 expression levels between these two, we found a significant ($p<0.05$; Wilcoxon test) increase of GREM1 expression in the pathologic/desmoplastic stromata

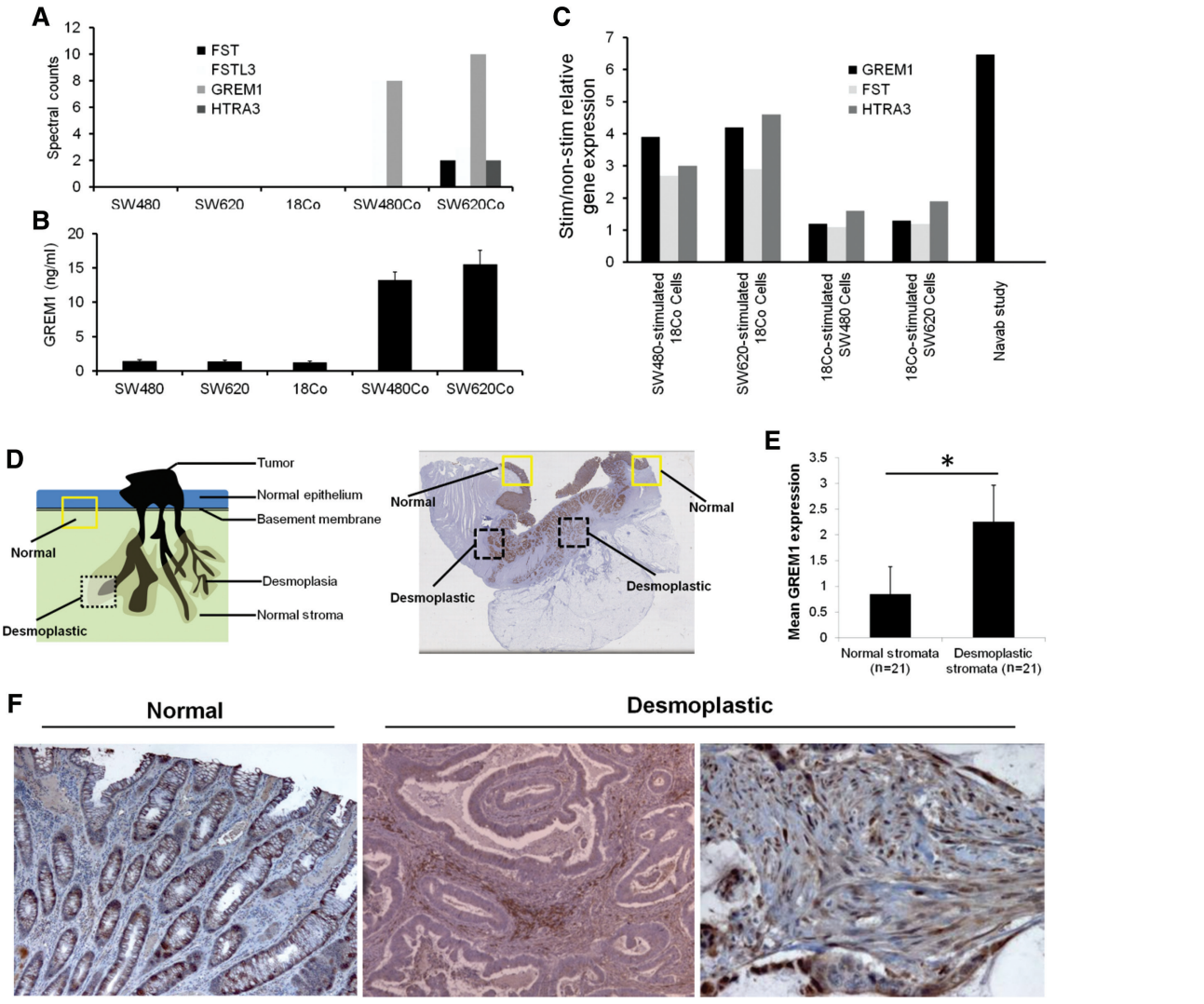

Figure 2 Gremlin-1 is expressed in the desmoplastic tumor-host cell interface of colorectal cancer.
(A) Normalized spectral counts of GREM1, FST, FSTL3 and HTRA3, four BMP suppressors/antagonists, in three monoculture supernatants (SW480, SW620, 18Co) and the respective coculture supernatants (SW480/18Co and SW620/18Co). Proteomic data for this analysis were derived from our previous study (Karagiannis et al., 2012a). (B) GREM1 protein levels were assessed in conditioned media, after recapitulating the experimental conditions described in our previous study (Karagiannis et al., 2012a). Note that only basal levels of GREM1 were detected in monoculture supernatants using a specific GREM1 immunoassay. (C) Relative GREM1, FST and HTRA3 gene-expression levels in indirect cocultures (stimulation with conditioned media). The last bar in the graph depicts differences in GREM1 expression levels between cancer-associated fibroblasts and normal fibroblasts in the Navab study (Navab et al., 2011). Bars demonstrate fold-difference of GREM1 gene expression in stimulated versus non-stimulated cells. Asterisks denote statistical significance, $p<0.05$, Mann-Whitney U-test. (D) Schematogram and proof-of-concept immunohistochemical figure (β-catenin), explaining the design of the immunohistochemical study, showing the areas from which normal and pathologic stromata were selected for further scoring. (E) Mean expression score of GREM1, as assessed through immunohistochemistry in pathologic and normal stromata of CRC patients. Asterisk denotes statistical significance, $p<0.05$, Wilcoxon test. (F) IHC snapshots from 1 CRC patient, demonstrating prominent difference in the stromal expression of GREM1 between normal and pathologic interfaces. Note the slight GREM1 expression around the colonic epithelium (mucosa), corresponding to the pericryptal myofibroblasts, and serving as positive control. All original magnifications ×200; except for the last ×400.

(Figure 2E), further indicating that GREM1 secretion in the tumor microenvironment is primarily elicited in the desmoplastic response. One prominent example of increased GREM1 expression in CAFs as opposed to adjacent healthy tissue is illustrated in Figure 2F.

GREM1 is contextually secreted in desmoplastic interface with EMT-pertaining phenotype

The downward margins of epithelial tumors are characterized by dedifferentiation, local invasion and migration

of cancer cells, while the surrounding stroma is conceptualized as a niche-supportive source (Sneddon and Werb, 2007). In such areas, EMT-promoting factors dominate over the EMT-suppressive ones, and are believed to render self-renewal and other malignant properties to the cancer cells (Scheel and Weinberg, 2012). Interestingly, the BMP pathway has been implicated in the regulation of differentiation equilibriums in a variety of contexts and epithelial-mesenchymal interactions, such as in the maintenance of stem cell niches in the bottom of healthy intestinal crypts (He et al., 2004; Ishizuya-Oka, 2005; Kosinski et al., 2007). To support the notion that GREM1 may also identify as a niche factor, we made observations in patient tissues, whereby we examined the relationship between stromal GREM1 expression and EMT induction. We extended our observations in three distinct areas of cancer invasion, namely the submucosal invasion fronts (SIFs), the isolated tumor nests (TNs), and areas of deep cancer invasion, such as cancer cell cohorts invading the muscularis externa (IIFs).

Our initial observations were made in areas where cancer cells have already penetrated the muscularis mucosa and invade into the submucosal connective tissue in a finger-like projection pattern (Figure 3A; middle panel), here referred to as SIFs. Histologically, the EMT-pertaining SIFs significantly differed from the EMT-quiescent ones, with most striking difference the absence of pseudoglandular formation and the poor differentiation in the former ones (Figure 3A). Notably, the EMT-pertaining contexts appeared in the form of tumor-budding in many cases, which are small groups of one to five cancer cells that have detached from the invasion front (Zlobec and Lugli, 2011; Mitrovic et al., 2012). Either reflecting to EMT-pertaining or EMT-quiescent, all the areas selected bore a purely desmoplastic microenvironment as assessed by the prominent co-expression of α-SMA/LAMB1 and absence of h-CALD to exclude the possibility of smooth muscle cell invasion (Figure 3B). However, GREM1 was more significantly ($p<0.05$; Mann-Whitney *U*-test) expressed in the EMT-pertaining areas, when compared to the EMT-quiescent ones (Figure 3B,C). Figure 3D demonstrates the pseudoglandular formation of the cancer cell cohort, the moderate-to-well differentiation of individual cancer cells, the membranous expression of β-CAT and the strict expression of OCLN in tight junctions (white arrows) in the GREM1-negative EMT-quiescent SIF, contradicting it at the same time with the loss of glandular appearance, the poor differentiation, the strong nuclear translocation of β-catenin and the absent-to-low OCLN immunoreactivity in the GREM1-positive EMT-pertaining SIF.

We performed a relevant analysis in TNs, which are invasive fronts characterized by isolated multicellular aggregates, possibly detached from larger cancer cell cohorts invading the stroma (Figure 4A). These TNs might be associated with a passive, invasion-independent metastatic pathway, initiated by their intravasation after getting enveloped by endothelial cells of sinusoidal vasculature (Sugino et al., 2002, 2004; Kukko et al., 2010). A careful observation of the 42 selected TNs revealed that the cancer cell cohorts were circumscribed by ECM-enriched envelopes, whose structure was possibly of a combination of desmoplastic and sinusoidal nature. Specifically, they were positive for LAMB1, and remarkably circumscribed by very thin α-SMA-positive and h-CALD-positive sheath (Figure 4B; yellow arrows). Most of these TNs (n=31) presented with prominent OCLN and β-CAT gradients (Figure 4C; upper panels), however a few (n=11) were categorized in the EMT-quiescent phenotype. Stromal GREM1 expression around these TNs was mild and variable in most cases, but focal expression in a few cancer cells in their periphery was also prominent (Figure 4B). We found that GREM1 expression was significantly higher ($p<0.05$; Mann-Whitney *U*-test) around EMT-pertaining compared to EMT-quiescent areas (Figure 4C).

As explained, IIFs are characterized by collective invasion/migration of cancer tissue into the muscularis externa in an interdigital pattern (Figure 5A). Careful observation of 28 selected IIFs revealed that cancer cell cohorts were circumscribed by ECM-enriched sheaths of low-to-medium thickness. These ECM-enriched sheaths were of myofibroblastic/CAF nature, as they retained the typical signature of LAMB1+/α-SMA+/h-CALD- (Figure 5B). Therefore, these cohorts do not come in direct contact with smooth muscle tissue, but they seem to migrate alongside CAFs. Two additional hallmarks of desmoplastic reaction were present in these sheaths. First, the myofibroblastic cells focally expressed the marker of proliferation Ki-67 (Figure 5B). Indeed, it is known that desmoplasia is not only characterized by abundant deposition of ECM components but also by the molecular recruitment and proliferation of myofibroblasts around cancer cells (Kunz-Schughart and Knuechel, 2002a). Second, there was a prominent population of $CD31^+$ cells (Figure 5B). This finding may suggest that increased angiogenesis is invoked within these migratory regions, through mechanisms by which CAFs secrete proangiogenic factors (Orimo et al., 2005; Watnick, 2012). In addition, the scattering pattern of these $CD31^+$ cells implies the deployment of a *de novo* angiogenic program in this area, rather than invasion of such enormous cancer cell cohorts in pre-existing blood vessels. GREM1 expression

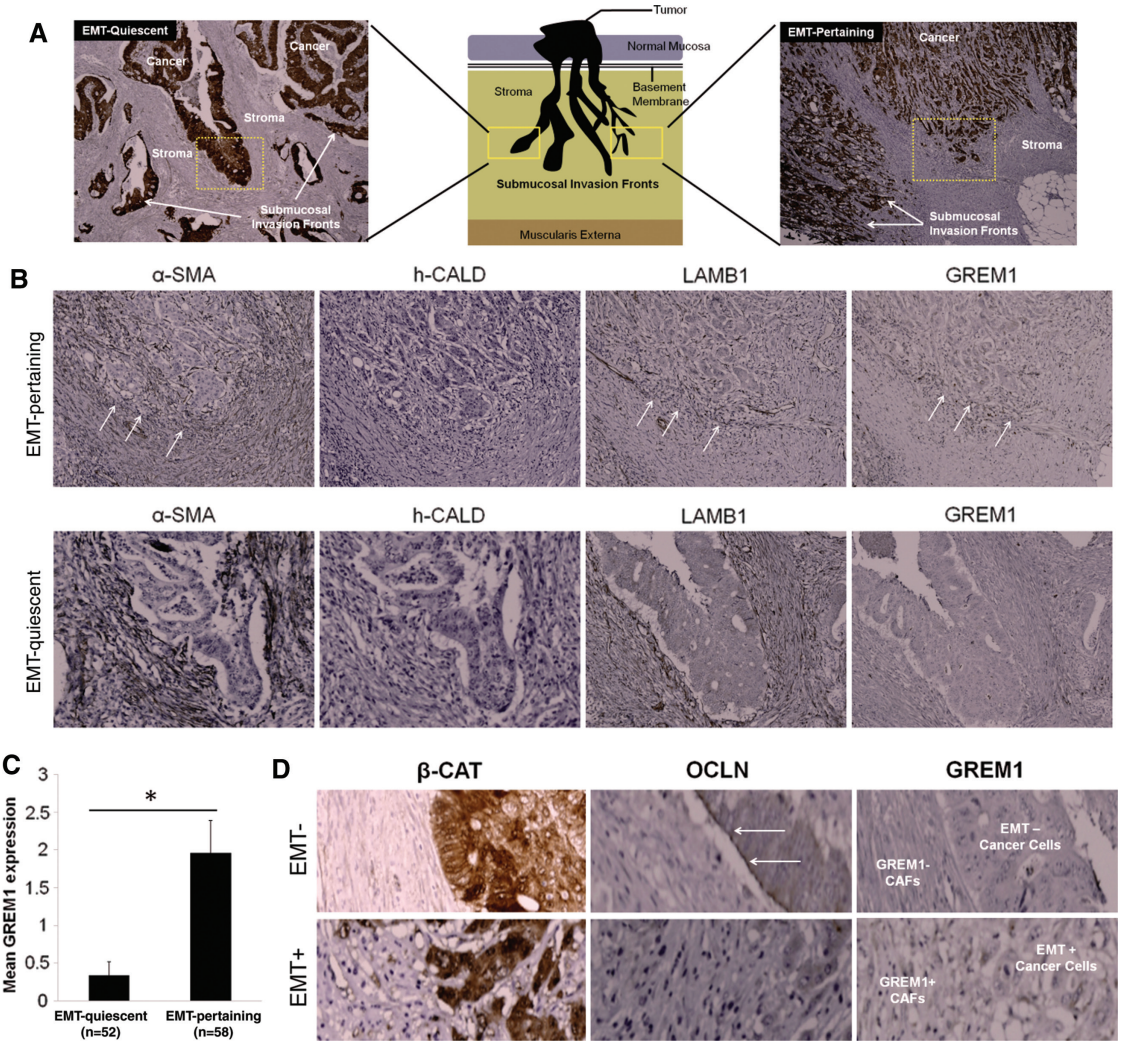

Figure 3 Association of GREM1 expression with EMT in submucosal invasion fronts (SIFs). (A) Illustration explaining the selection of SIFs. The cartoon on the middle demonstrates the design of selection, while the figures on the left and right demonstrate examples of SIFs (β-CAT staining), with the left being an EMT-quiescent, while the right being an EMT-pertaining one. Original magnifications ×40. (B) Set of figures of the two selected areas shown in panel A, indicating the staining of each of the specified markers. In both EMT-pertaining and EMT-quiescent snapshots, the peritumoral stroma is characterized by the desmoplastic signature (α-SMA+/LAMB1+/h-CALD-). Note that GREM1 immunoreactivity is noted in the EMT-pertaining SIF only. White arrows indicate immunoreactivity of the specified marker. All original magnifications ×200. (C) Mean GREM1 expression score between EMT-pertaining and EMT-quiescent SIFs. Asterisk indicates $p<0.05$; Mann-Whitney *U*-test. (D) Topographic association of GREM1 expression with EMT. The EMT-quiescent SIF (upper set of figures) demonstrates the following characteristics: membranous staining of β-CAT, strong OCLN expression in tight junctions (white arrows) and absence of GREM1 immunoreactivity in the desmoplastic stroma. The EMT-pertaining SIF (lower set of figures) demonstrates the following characteristics: nuclear staining of β-CAT, loss of OCLN expression from the tight junctions and focal GREM1+ in both the stromal and the epithelial compartment of the tumor. All original magnifications ×400.

in these desmoplastic sheaths was variable but detectable in most cases (Figure 5B). We compared the expression levels of GREM1 in IIFs and found that GREM1 expression was significantly higher ($p<0.05$; Mann-Whitney *U*-test) around EMT-pertaining compared to EMT-quiescent areas (Figure 5C).

GREM1 has been recently linked to the regulation of angiogenesis in a BMP-independent/VEGFR-dependent mechanism, in both healthy and neoplastic states (Stabile et al., 2007; Mitola et al., 2010; Chen et al., 2012; Mulvihill et al., 2012; Ravelli et al., 2012). Interestingly, our immunohistochemical observations suggested that GREM1+ desmoplastic microenvironments were also angiogenic (i.e., Figure 5B). The potential of CAFs in eliciting angiogenic responses through SDF1/CXCL12 and/or VEGF secretion has been well-documented (Kunz-Schughart and

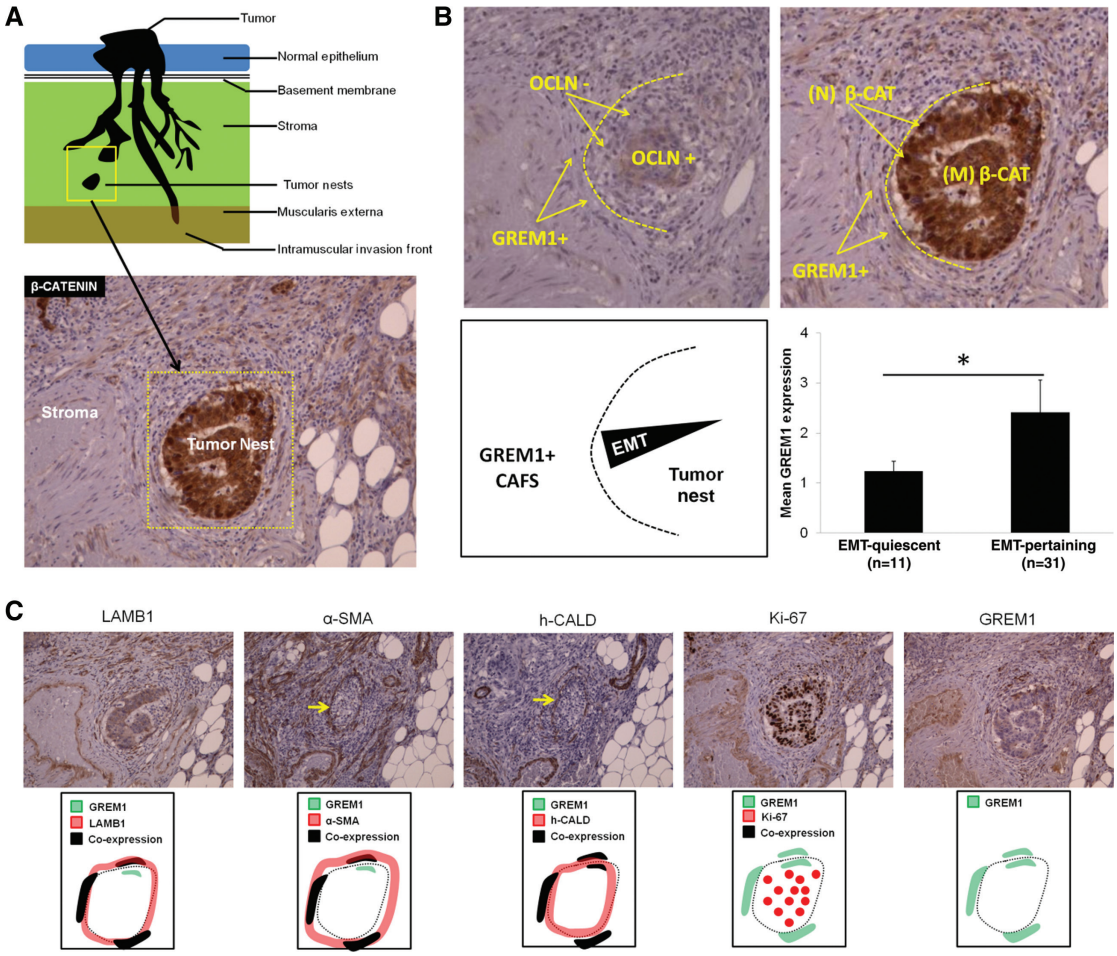

Figure 4 Association of GREM1 expression with EMT in isolated tumor nests (TNs).
(A) Illustration explaining the selection of TN areas. The upper cartoon illustration demonstrates the design of selection, while the figure below demonstrates an example of TN (β-CAT staining). Original magnification ×250. (B) Topographic association of GREM1 expression with EMT. The EMT-pertaining cancer cell cohorts of the TNs demonstrate prominent EMT gradation with the following characteristics: focal nuclear staining of β-CAT in the periphery with parallel membranous expression in the core of the cells (right panel) and progressive loss of OCLN from the core to the periphery of TNs (left panel). The cartoon schematic in the low-left corner shows the gradation of the EMT process, as implied from the panels above. The graph in the low-right corner demonstrates statistically significant difference of GREM1 expression in the TN envelopes between EMT-pertaining and EMT-quiescent TNs. Asterisk indicates $p<0.05$; Mann-Whitney *U*-test. All original magnifications ×300. (C) Set of figures of the selected TN shown in panel (A), indicating the staining of each of the specified markers (panel above) and a cartoon illustration (panel below), which demonstrates topographical overlap of the expression of the corresponding protein with that of GREM1. GREM1 is mildly expressed in stromal cells comprising the envelope and focally by cancer cells at the periphery of these TNs. The TN envelopes are LAMB1+, and remarkably have very thin α-SMA+ and h-CALD+ layer around them (yellow arrows). All original magnifications ×200.

Knuechel, 2002b; Orimo et al., 2005). We exploited the possibility that GREM1 might serve as an alternative angiogenesis mediator. To achieve so, we compared GREM1 protein expression levels between hypo- and hypervascularized stromata (Figure 6A). A total of 168 invasive fronts were selected in an unbiased way by using the β-CAT stain and they were scored for stromal GREM1 expression. These areas were then mapped to the endothelial marker CD31, from which the pixilated areas corresponding to immunoreactivity were calculated in a software-assisted fashion, and were subsequently ranked with increasing score to get categorized into densely-angiogenic (high-CD31) or sparsely-angiogenic (low-CD31) areas, using the median as cut-off (Figure 6B). Interestingly, there was a significant increase ($p<0.05$; Mann-Whitney *U*-test) in the mean GREM1 expression in high-CD31 compared to low-CD31 areas (Figure 6C). However, we noticed that endothelial cell recruitment is not necessarily

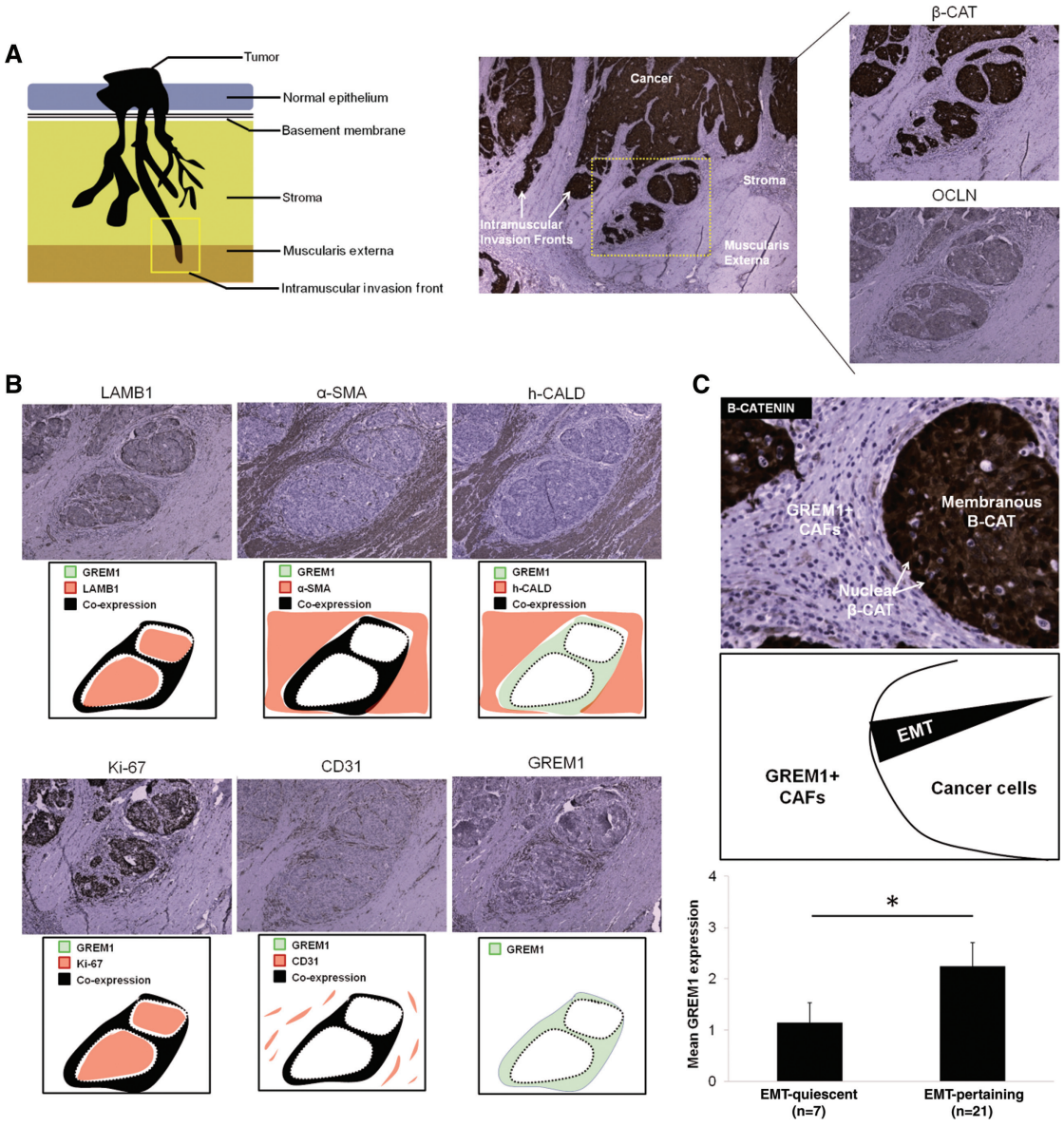

Figure 5 Association of GREM1 expression with EMT in intramuscular invasion fronts (IIFs).
(A) Illustration explaining the selection of IIFs. The cartoon on the left demonstrates the design of selection, while the figure on the middle demonstrates an example of IIF (β-CAT staining). The demarcated yellow-squared area is further shown magnified (original magnification ×200) with both β-CAT and OCLN staining on the far right. (B) Set of figures of the selected IIF shown in panel A, indicating the staining of each of the specified markers (panel above) and a cartoon illustration (panel below), which demonstrates topographical overlap of the expression of the corresponding protein with that of GREM1. GREM1 is expressed in the thin desmoplastic, peritumoral sheath, as the cancer cell cohorts invade into the muscularis externae. This sheath is LAMB1+, α-SMA+ and h-CALD- (upper panels). The desmoplastic sheath is especially distinguished easily in the h-CALD panel, as a thin layer between cancer and muscle cells. Also, the cancer cells and their peritumoral stroma show some variable degree of proliferation (Ki-67 staining), while the peritumoral sheath is focally CD31+, indicating increased angiogenesis. All original magnifications ×200. (C) Topographic association of GREM1 expression with EMT. The EMT-pertaining cancer cell cohorts of the IIFs demonstrate prominent EMT gradation with the following characteristics: nuclear staining of β-CAT in the periphery with parallel membranous expression in the core of the cells (upper panel). The cartoon schematic shows this gradation of the EMT process, as implied from the differential localization of β-CAT staining in such cancer cell cohorts (middle panel). The graph demonstrates statistically significant difference of GREM1 expression in the desmoplastic sheaths between EMT-pertaining and EMT-quiescent IIFs. Asterisk indicates $p<0.05$; Mann-Whitney *U*-test. Original magnification ×400.

accompanied by structuring into tubes (i.e., vasculogenesis), and as such, it is quite unclear whether these CD31$^+$ cells are indeed endothelial cells that are transforming into cancer-associated endothelium or are endothelial cells that undergo endothelial-to-mesenchymal transition (Zeisberg et al., 2007). In each case, peritumoral stromata

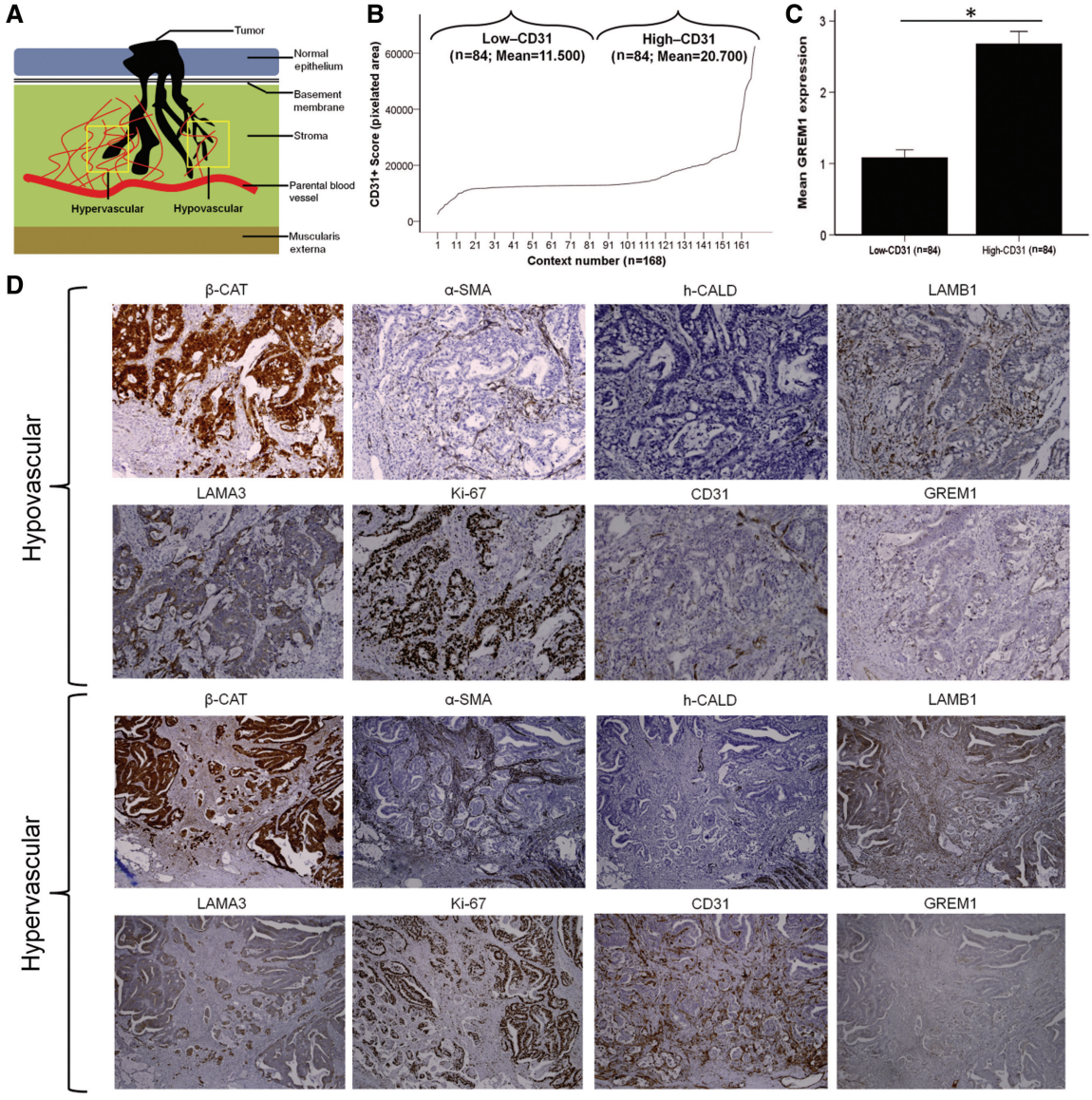

Figure 6 Association of GREM1 expression with hypervascular invasion fronts (HIFs).
(A) Cartoon illustration explaining the selection of hypovascular and hypervascular invasion fronts (HIFs). (B) Ranking of 168 selected areas with increasing vascular intensity, according to their CD31 expression score, as calculated through the pixilated area in a computer-assisted fashion. The median of CD31 expression score was used as a cut-off to divide the selected areas into hypervascularized (high-CD31) and hypovascularized (low-CD31) invasion fronts. (C) Mean GREM1 expression score between hypo- and hypervascularized invasion fronts (i.e., low-CD31 vs. high-CD31). Asterisk demonstrates $p<0.05$; Mann-Whitney *U*-test. (D) Set of figures from representative hypovascularized (upper set of figures) or hypervascularized (lower set of figures) areas, indicating the staining of each of the specified markers (i.e., α-SMA/LAMB1/h-CALD, β-CAT, LAMA3, Ki-67 and CD31), along with GREM1. Note that GREM1 staining is more focal in the hypovascularized, while a mild GREM1 blushing dominates both epithelial and stromal compartments in the hypervascularized areas. All original magnifications ×200.

of both hypo- and hypervascular invasion fronts were characterized by aberrant desmoplasia and absence of LAMA3 immunoreactivity (Figure 6D). GREM1 was only expressed focally in the hypovascular invasion fronts, whereas it tended to dominate the entire tumoral and peritumoral compartment (i.e., mild blush) in hypervascular states (Figure 6D).

The BMP7-GREM1 axis triggers the EMT switch to regulate cancer cell phenotype

Overall, the presented immunohistochemical data correlate the increased GREM1 expression in CAFs with the occurrence of an EMT phenotype in carcinoma cells of the desmoplastic interface. Along with supportive literature

evidence (Michos et al., 2004; Kosinski et al., 2007; Sääf et al., 2007), which collectively indicates that GREM1 has been causatively associated with the occurrence and maintenance of the mesenchymal phenotype in a number of developmental processes, as well as in mesenchymal and cancer stem cell niches, we sought to investigate through *in vitro* assays whether our observed correlations in the immunohistochemical studies reflect to causation.

First, phenotypic EMT assays were performed in HT29 colon cancer cells, as their ability to grow in colonies and their relatively well-differentiated phenotype (Ahmed et al., 2013) could provide safe assessment of an active EMT process. In addition, this cell line has been used for EMT studies in the past (Cai et al., 2013), which provided guidance for the current investigations. Morphological assessment of the epithelial/mesenchymal phenotype ratio in BMP7/GREM1 stimulation assays revealed that the addition of GREM1 alone, or in combination with BMP7, was able to cause some degree of disruption of cell-to-cell adhesion in HT29 colonies, and promoted the mesenchymal phenotype, especially in cancer cells that lined the periphery of the colonies (Figure 7A). Quantification with blinded observers demonstrated a significant decrease ($p<0.05$, Jonckheere-Terpstra test) in the percentage of cells with epithelial phenotype after treatment with GREM1 in a dose-dependent fashion (Figure 7B; upper panel). This remained significant even with the parallel administration of 50 ng/ml of BMP7 (Figure 7B; upper panel). However, the addition of BMP7 alone did not significantly affect the epithelial phenotype or ability of HT29 cells to form their typical cohorts/colonies (Figure 7A), an observation that further strengthens the notion that BMP7 promotes the integrity and maintenance of the epithelial phenotype (Motoyama et al., 2008). As subjective to a certain extent, these results were further confirmed through computer-assisted determination of cell circularity index (Figure 7B; lower panel), as previously described (Shen et al., 2014). In particular, the mean circularity index of HT29 cells was significantly reduced ($p<0.05$; Jonckheere-Terpstra test), following treatment with either GREM1 alone or combination of GREM1 and BMP7, and remained intact ($p>0.05$, Jonckheere-Terpstra test) following treatment with BMP7 alone (Figure 7B; lower panel).

Second, we determined the transcription status of two independent EMT machineries, the cadherin switch (i.e., simultaneous overexpression of the epithelial E-cadherin and downexpression of the mesenchymal N-cadherin) and EMT-promoting transcription factors, such as Snail-1 (Tse and Kalluri, 2007; Kalluri, 2009; Kalluri and Weinberg, 2009). During assay optimization, we noted that stimulation with TGF-β (5 ng/ml), a cytokine known to induce EMT in CRC and other cancers (Bates and Mercurio, 2005), was able to induce the cadherin switch and Snail-1 overexpression (data not shown), thus confirming previous studies (Li et al., 2010; Cai et al., 2013; Hirakawa et al., 2013) that have established the HT29 cell line as a model system for studying EMT induction. We then noticed that stimulation of HT29 cells with BMP7 alone caused a significant ($p<0.025$, Holms-corrected Jonckheere-Terpstra test) shift of the cadherin switch towards a non-EMT phenotype, in a dose-dependent fashion (Figure 7C). Moreover, stimulation with GREM1 alone caused a small, but significant ($p<0.025$, Holms-corrected Jonckheere-Terpstra test) shift towards the EMT phenotype, in a dose-dependent fashion (Figure 7C), confirming that the BMP7/GREM1 axis could regulate EMT. However, the fact that the cadherin switch was not altered severely by GREM1 stimulation alone (E-cadherin was decreased by ~1.3-fold, while N-cadherin was increased by ~1.8-fold with a single dose of 1000 ng/ml GREM1) prompted us to speculate that there may not be adequate levels of endogenously-secreted BMP7 in this *in vitro* setting. Let alone, most studies that have induced EMT in HT29 cells have observed significant results in ~8 days post stimulations, and our experiments were terminated in 2 days post-treatment. To circumvent this issue, we investigated the effect of GREM1 stimulation after co-stimulation with 50 ng/ml of BMP7. In this case, we again observed a statistically significant ($p<0.025$, Holms-corrected Jonckheere-Terpstra test) shift of the cadherin switch towards the EMT phenotype (Figure 7C). This particular experiment was also verified at the protein expression level, in which E-cadherin reduction was very prominent, while N-cadherin increase occurred slower and to a less extent, following the administration of GREM1 in a dose-dependent manner in HT29 cells (Figure 7D).

Coincidentally, the gene-expression level of the EMT-initiating transcription factor Snail (SNAI1) was inversely correlated with BMP7 ($p<0.05$, r=-0.46; Spearman's correlation coefficient), when all possible correlations with the BMPs were tested (Figure 7E). Mean levels of Snail gene expression were higher in cancerous lesions compared to normal colonic mucosa in the CRC-patient cDNA array (Figure 7F, Figure S3I). On this basis, when we stimulated HT29 cells with increasing doses of either BMP7 (0.5, 5 and 50 ng/ml) or GREM1 (10, 100 and 1000 ng/ml), we observed significantly lower expression of SNAI1 in the former, and significantly higher expression of SNAI1 in the latter case (both were shown with $p<0.05$, Holms-corrected Jonckheere-Tersptra test) (Figure 7G). Concordantly, a dose-dependent SNAI1 overexpression ($p<0.05$, Holms-corrected Jonckheere-Tersptra test) was also observed in HT29 cells treated with a single dose of 50 ng/ml of BMP7, following increasing doses of GREM1 (10, 100

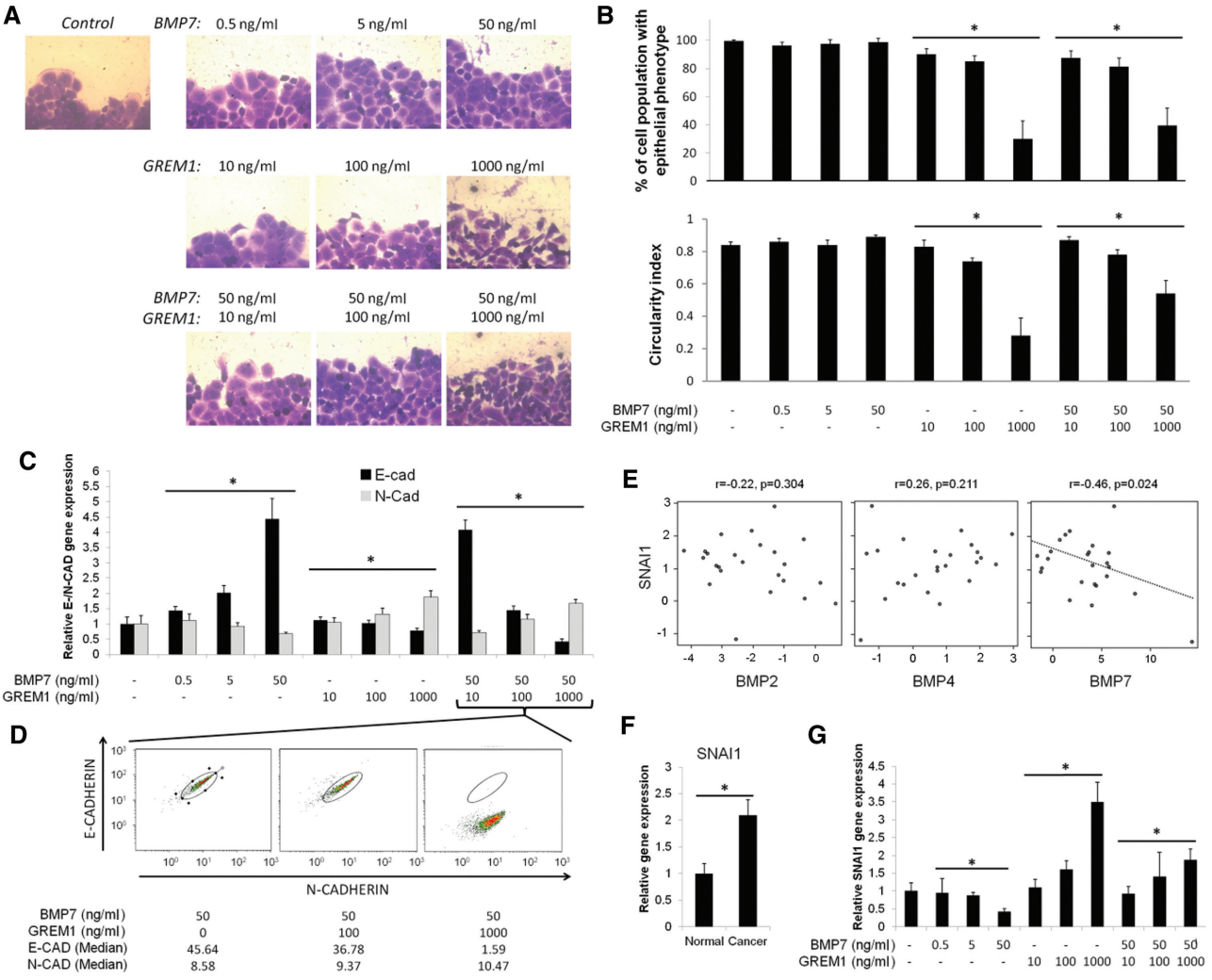

Figure 7 Regulation of EMT by the BMP7/GREM1 axis *in vitro*.
(A) Representative snapshots of HT29 cells, after stimulation with varying doses of BMP7 (0.5, 5 and 50 ng/ml), GREM1 (10, 100 and 1000 ng/ml) or both (BMP7 at 50 ng/ml; GREM1 at 10, 100 and 1000 ng/ml). All original magnifications ×400. (B) Mean percentage of cell population with an epithelial phenotype (upper graph) and mean circularity index (lower graph) of each of the experimental conditions demonstrated in panel (A). Asterisks denote statistical significance, $p<0.05$, Jonckheere-Terpstra test. (C) Mean gene-expression levels of E-cadherin and N-cadherin, after recapitulating the experimental conditions demonstrated in panel (A). All bars indicate relative E- and N-cadherin expression values to the respective non-treated control. Asterisks denote statistical significance, $p<0.007$, Jonckheere-Terpstra test. (D) Flow cytometry of HT29 cells treated with a single dose of 50 ng/ml BMP7 and increasing doses of GREM1 (from left to right: 10 ng/ml, 100 ng/ml and 1000 ng/ml). (E) Scatter plots demonstrating correlation between the gene-expression levels of SNAI1 and each one of the three major BMPs (BMP2, BMP4 and BMP7) in CRC patients (cDNA array). Statistical significance is shown with $p<0.05$, Spearman's Ranked Correlation test. (F) Relative gene-expression levels of SNAI1 between cancer lesions and adjacent healthy areas of CRC patients (cDNA array). Asterisk denotes statistical significance, $p<0.007$, Wilcoxon test. (G) Mean gene-expression levels of Snail (SNAI1) in HT29 cells, after recapitulating the experimental conditions demonstrated in panel (A). All bars demonstrate relative values to the non-treated control. Asterisks denote statistical significance, $p<0.007$, Jonckheere-Terpstra test.

and 1000 ng/ml) (Figure 7G). However, the comparative SNAI1 expression values in BMP7/GREM1-treated HT29 cells were lower than those of GREM1 alone (Figure 7G), an observation which confirms (along with all the data presented in this section) that GREM1 probably antagonizes BMP7 to induce EMT, at least in this *in vitro* model system.

Discussion

In our previous review (Karagiannis et al., 2010), we mentioned that the cancer secretome has significant potential for diverse applications in oncoproteomics. Such proteins might represent putative tumor biomarkers or therapeutic targets. Consequently, proteomic strategies for secretome

analysis have been extensively deployed over the past few years. These efforts generated a large amount of information awaiting deeper mining and careful interpretation. By combining secretome data from multiple CRC cell line monocultures, as well as from cocultures, we defined a secreted signature of BMP antagonists, as key element of CRC progression. We demonstrated that the BMP antagonist GREM1 is contextually expressed by CAFs in the colon cancer microenvironment, and may promote EMT *in vitro*.

In CRC, BMP signaling has been regarded as generally portraying tumor-suppressive capabilities, such as reducing cancer cell proliferation, invasion, motility, and antagonizing EMT (Bendtsen et al., 2004; Nishanian et al., 2004; Beck et al., 2006, 2007; Beppu et al., 2008; Wu et al., 2008; Bertrand et al., 2012). Remarkably, a wide range of tumor-promoting features has also been reported (Deng et al., 2007a,b; Grijelmo et al., 2007; Kang et al., 2009; Lorente-Trigos et al., 2010). These seemingly conflicting observations support the notion that the BMP pathway affects cancer progression depending on cell type and context. For instance, Owens et al. demonstrated that disruption of BMP receptor type II (BMPR2) in breast tumor cells may promote metastasis, through increased tumor cell proliferation, invasion, migration and EMT (Owens et al., 2011). Interestingly, the same group reported that an active BMP signaling in CAFs may enhance mammary carcinoma cell invasion (Owens et al., 2013).

Carcinomas are multifaceted tissues, and they not only comprise of tumor cells but also of a wide variety of stromal cells, including fibroblasts, immune and endothelial cells among others, as well as components of the extracellular matrix. Paracrine interactions between those and carcinoma cells may assist in the development and progression of cancer (Bissell and Radisky, 2001; Elenbaas and Weinberg, 2001; Bhowmick and Moses, 2005; Hanahan and Weinberg, 2011). Our IHC observations demonstrated strong expression of the BMP antagonist GREM1 in CAFs of the invasion front. Cancer cells in such areas deploy a specialized molecular and pathological EMT signature (De Wever et al., 2008), which may be responsible for local invasion and their detachment in form of small cohorts, known as 'tumor-buds' (Karagiannis et al., 2014c). To which extent, CAF-triggered BMP antagonism may facilitate the process of tumor-budding remains to be elucidated.

Using *in vitro* EMT assays, based on the expression of the EMT-initiating transcription factor *Snail* and the 'cadherin switch', we have shown that BMP7 promoted cancer cell differentiation (i.e., inhibition of EMT), and that GREM1 could antagonize this effect. Despite clear evidence from developmental studies, the regulation of cell differentiation in the cancer setting has been a subject of major speculation for the BMP pathway (Chen et al., 2004; Gazzerro and Canalis, 2006; Bertrand et al., 2012). Such debates have arisen due to the documented difficulty of studying the role of the BMP pathway in cancer progression, as there is: (a) a broad spectrum of BMP ligands/receptors/antagonists in the tumor microenvironment which may compensate for one another and which may or may not be interconnected under the same downstream pathway; (b) a wide variety of canonical/non-canonical downstream effects; (c) heterogeneous regulation of their expression profile; and (d) a complicated intracellular interactome of the signaling relay from the receptor level down to the transcription factor/co-regulator level (Chen et al., 2004; Gazzerro and Canalis, 2006; Bertrand et al., 2012).

It has been suggested that GREM1 preferentially shifts the differentiation state of cancer cells toward a more mesenchymal and stem-like phenotype, which may also promote their maintenance within tumor hierarchy (Sneddon et al., 2006; Yan et al., 2014). In contrast, BMPs may trigger and promote the differentiation of stem cells in many settings (Xu et al., 2005; Kosinski et al., 2007; Zhang et al., 2011). As such, our current observations support a more generic hypothesis that BMP antagonists may define a niche for a self-renewing population in certain cancers (Sneddon and Werb, 2007). Actually, recent evidence has connected the acquisition of cancer stem cell (CSC) (or cancer-initiating cell) traits, following an EMT program (Alison et al., 2012; Scheel and Weinberg, 2012). The current study is not intended, at this point, to bridge the space between CSCs and EMT-pertaining invasion fronts, as being the exact same cancer subpopulation, despite the fact that this notion has already been suggested in the 'hallmarks of cancer' (Hanahan and Weinberg, 2011). The origins of CSCs within a solid tumor have not yet been clarified, and may well vary from one tumor type to another. However, the induction of the EMT program in certain model systems is sufficient by itself to provide 'stemness' in the target population, including the characteristics that define the stem-like phenotype, i.e., self-renewal capability and specific antigenic properties. Such notion may not only suggest that the EMT program can enable cancer cells to physically disseminate from primary tumors, but also confer self-renewal ability on them, which may be crucial for clonal expansion (Brabletz et al., 2005; Spaderna et al., 2007). Therefore, upon generalization, this connection raises a corollary model: the heterotypic signals that trigger EMT, such as those released from the desmoplastic stroma (i.e., GREM1), could be sufficient and/or necessary for creating and maintaining CSC niches (Sneddon and

Werb, 2007; Sell, 2010; Scheel and Weinberg, 2012; Yan et al., 2014).

Besides being noticed in the desmoplastic context, GREM1-mediated inhibition of BMP7 has also been reported in pulmonary fibrosis (Myllärniemi et al., 2008), diabetic nephropathy (Lappin et al., 2002; Murphy et al., 2002) and pauci-immune glomerulonephritis (Mezzano et al., 2007). Therefore, GREM1 might have a more generic function in the adult organism, by supporting and regulating fibrosis of diseased tissues.

Given the reported BMP signaling pathway cross-talk and non-canonical signaling relays (von Bubnoff and Cho, 2001), it should be mentioned that the exact downstream signaling events were not elucidated in the current study. Additionally, in many cases CRC undergoes a molecular pathway that causes genetic instability in microsatellite loci attributable to alterations in the DNA mismatch repair genes, such as *MLH1*, *MSH2*, *MSH6* and *PSM2* (Ilyas et al., 1999; Markowitz and Bertagnolli, 2009; Boland and Goel, 2010). This molecular pathway has been shown to affect many canonical signal transduction pathways through genetic silencing because of the high frequency of mutations, such as the TGF-β superfamily pathways (Ilyas et al., 1999). In such cases, BMPs may signal through non-canonical downstream pathways. As such, the downstream effects of the newly reported BMP7/GREM1 axis should be investigated with caution. However, our stimulation experiments were performed in HT29 cells, a microsatellite stable colon adenocarcinoma cell line, capable of producing carcinoembryonic antigen (von Kleist et al., 1975). Therefore, our subsequent co-stimulation assays, where HT29 cells were co-treated with a single dose of BMP7 and varying doses of GREM1, suggest that the BMP7/GREM1 axis might also signal through the canonical pathway.

Our immunohistochemical observations additionally demonstrated focal GREM1 staining in TNs, possibly reflecting areas of vascular invasion. Vascular invasion comprises a unique model of migration-independent metastasis, according to which TNs/buds are dynamically and passively enveloped by the sinusoidal cancer-associated endothelium (Sugino et al., 2004). Our studies have demonstrated that GREM1 is present in this remodeled endothelium, further suggesting that it could potentially participate in vascular remodeling and intravasation of tumor emboli within the vessels. In a supportive fashion, GREM1 has been previously associated with angiogenesis in a BMP-independent fashion (Stabile et al., 2007; Mitola et al., 2010).

Future efforts should encompass understanding of the causative implication of GREM1-mediated BMP disruption in CRC metastasis, using relevant *in vivo* models. $GREM1^{-/-}$ mice have been utilized in a number of developmental studies, but die of complete renal agenesis shortly after birth (Khokha et al., 2003; Michos et al., 2007), an issue that renders this background inappropriate for studying CRC. However, it has been shown that heterozygous $GREM1^{+/-}$ mice are both viable and healthy, can grow normally and show no differences from wild type $GREM1^{+/+}$ mice or vulnerability to any disease (Roxburgh et al., 2009). This animal model has been successfully used to study the implication of GREM1 in diabetic nephropathy (Roxburgh et al., 2009), and could be utilized in our context.

In summary, we have reported a possible implication of GREM1 with CRC progression. Our tissue-expression and *in vitro* studies converge to the preferential expression of GREM1 in peritumoral stromal sheaths composed of CAFs. These GREM1-expressing CAFs may participate in a paracrine signaling conversation with the proximal invasion front, resulting in BMP-signal suppression and possibly EMT. To which extent this process could lead to local invasion and tumor-budding formation needs to be addressed in the future.

Materials and methods

Cell culture

The HT29 (HTB-38), SW480 (CCL-228), SW620 (CCL-227) and RKO (CRL-2577) colon cancer cell lines, as well as the normal colonic fibroblasts 18Co (CCD-18Co), were obtained from ATCC, Rockville, MD. Cells were maintained in their favorable growth medium, according to the manufacturer's instructions, in a modified atmosphere of 5% CO_2 in a humidified incubator at 37°C. All experiments were conducted within <3 passages from the initiation of all cultures.

Gene-expression analysis of BMP signaling components using real-time PCR

The TissueScan Colon Cancer cDNA Array III was used (Origene, Rockville, MD) for determining gene-expression levels of members of the BMP pathway in a commercially available cohort of CRC patients. This array consists of CRC tissues from 24 patients, matched with normal colonic mucosal tissue adjacent to the tumor. For assessment of gremlin-1 expression in 'indirect' colon cancer cocultures, we stimulated cancer cells with fibroblast medium and vice-versa. Stimulation media (SW480, SW620 and 18Co) were collected under serum-free conditions, as previously described (Karagiannis et al., 2014a). Co-cultured cells were stimulated for 2 days with media containing 50% stimulation medium and 50% fresh medium. RT-PCR was performed by using 1X SYBR green reagent (Applied Biosystems, Burlington, ON) as previously described (Saraon et al., 2012, 2013), and transcript

Table 1 Forward and reverse (5′→3′) primers for RT-PCR.

Gene	Forward primer	Reverse primer
GAPDH	GTCTCCTCTGACTTCAACAGCG	ACCACCCTGTTGCTGTAGCCAA
BMP2	TGTATCGCAGGCACTCAGGTCA	CCACTCGTTTCTGGTAGTTCTTC
BMP4	CTGGTCTTGAGTATCCTGAGCG	TCACCTCGTTCTCAGGGATGCT
BMP7	GAGTGTGCCTTCCCTCTGAACT	AGGACGGAGATGGCATTGAGCT
BMPR1A	CTTTACCACTGAAGAAGCCAGCT	AGAGCTGAGTCCAGGAACCTGT
BMPR1B	CTGTGGTCACTTCTGGTTGCCT	TCAATGGAGGCAGTGTAGGGTG
BMPR2	AGAGACCCAAGTTCCCAGAAGC	CCTTTCCTCAGCACACTGTGCA
FST	AGCAGCCAGAACTGGAAGTCCA	CCGATTACAGGTCACACAGTAGG
GREM1	TCATCAACCGCTTCTGTTACGGC	CAGAAGGAGCAGGACTGAAAGG
HTRA3	CAAGAAGTCGGACATTGCCACC	CGTTGTCACTGTGTTCTGTAGGG
SNAI1	TGCCCTCAAGATGCACATCCGA	GGGACAGGAGAAGGGCTTCTC
E-CAD	GCCTCCTGAAAAGAGAGTGGAAG	TGGCAGTGTCTCTCCAAATCCG
N-CAD	CCTCCAGAGTTTACTGCCATGAC	GTAGGATCTCCGCCACTGATTC

levels of β-actin, BMP-2, -4, and -7, BMPR1A, -1B and 2, GREM1 and FST were measured on a 7500 ABI System. Forward (F) and reverse (R) primer sequences utilized for each gene are listed in Table 1.

GREM1 immunoassay

SW480, SW620 and 18Co cells were seeded in triplicates in 6-well plates (DMEM, 10% FBS), in mono- or cocultures (SW480Co/SW620Co) up to ~50–60% confluence, as described (Karagiannis et al., 2012a). CM from all wells were then replaced with 2 ml serum-free DMEM. CM were collected after 2 days and GREM1 concentration was measured with a commercially available immunoassay (Invitrogen), using the manufacturer's instructions.

Alkaline phosphatase assay

Alkaline phosphatase (ALP) activity was used to demonstrate active BMP signaling in various CRC cell lines, and was determined by para-nitrophenylphosphate (p-NPP) hydrolysis, as previously described (Souvannavong et al., 1995; Akcakaya et al., 2007). In brief, following the termination of BMP7 stimulation experiments, cancer cells were washed twice with PBS and cell viability was assessed by exclusion of 0.5% Trypan Blue dye (data not shown). Approximately 500 000 cells in each condition were centrifuged for 5 min at 750 *g*, and their supernatants were discarded. Then, the cell pellets were suspended in 100 ml substrate buffer (10 mM diethanolamine, 0.5 mM $MgCl_2$, pH 10.5), and 1 mg/ml p-NPP was added. The mixture was incubated for 20 min at room temperature. The reaction was stopped with 50 ml 2 N NaOH. Optical density (OD) was measured at 405 nm. The optimization experiment showed that treatment with increasing doses of BMP7, increased the ALP activity of HT29, SW480 and SW620 in a dose-dependent fashion, whereas RKO cells served as negative control (Figure S1). As such, we validated previous literature (Beck et al., 2006; Grijelmo et al., 2007; Deng et al., 2009; Kang et al., 2009) demonstrating that HT29, SW480 and SW620 cells could be used as an efficient *in vitro* model system for BMP signaling studies.

Morphological and computer-assisted assessment of EMT

HT29 cells were seeded in triplicate in 12-well plates (DMEM, 10% FBS), to ~50% confluence and were then stimulated with rhTGF-β (Sigma-Aldrich) or rhBMP7 (Sigma-Aldrich) or rhGREM1 (Sigma-Aldrich) or combinations for 2 days, under serum-free conditions. Evaluation of EMT incidence was performed through two independent methods: operator-subjective and computer-assisted. For the former, three wells per experimental condition were fixed in 4% paraformaldehyde and stained with 0.5% crystal violet, as described (Karagiannis et al., 2014a). Five snapshots from each well (to a total of 15 pictures per experimental condition) were given to four blinded observers for independently assessing the percentage of cell population with epithelial phenotype. Score values of each experimental condition were combined for all snapshots from all different observers in one final mean score per experimental condition. For the latter, one-well per experimental condition was subjected to circularity index analysis, using ImageJ. Based on pixel analysis of cell shape in a cell-by-cell basis, a perfect circle gives an index of 1.0, whereas the more polygonal, spindle-shaped or ellipsoid one shape is, the closer to 0.0 the index becomes. In brief, comparison of circularity indexes among the various experimental conditions was performed. For each condition, the circularity of approximately 120–150 individual cells was calculated, and a mean index was determined. As HT29 cells tend to grow in colony configuration *in vitro*, at least three independent colonies/areas were selected in each experimental condition for evaluating the circularity of the cells. According to one study using the method (Shen et al., 2014), it is presumed that cells with small circularity index are more mesenchymal, thus representing populations that have possibly undergone EMT.

Gene-expression analysis of EMT markers using real-time PCR

In addition to the morphological and computer-assisted assessment of EMT, the same experimental conditions were reproduced to assess specific EMT markers in the gene-expression level. As such, 2 days

after BMP7/GREM1 stimulation, HT29 cells were collected using non-enzymatic dissociation buffer (EDTA), and subjected to RNA extraction and cDNA synthesis, as previously described (Saraon et al., 2013; Karagiannis et al., 2014a). RT-PCR was performed using 1X SYBR green reagent (Applied Biosystems) and transcript levels of Snail (SNAI1), E-cadherin (CDH1) and N-cadherin (CDH2) were measured on a 7500 ABI System. Forward (F) and reverse (R) primer sequences utilized for each gene are listed in Table 1.

Flow cytometry

HT29 cells were cultured in 6-well plates (10^6 cells per well) to 75% confluence and subjected to stimulating conditions according to the question asked. Cells were detached using a non-enzymatic EDTA-based cell dissociation buffer and suspended in 0.5 ml PBS, fixed for 10 min at 37°C to a final concentration of 4% formaldehyde and eventually chilled on ice for 1 min. Following that, cells were aliquoted into 100 µl of incubation buffer (PBS, 0.5% BSA) and AF647-E-CAD [E-cadherin (24E10) Rabbit mAb (Alexa Fluor 647 Conjugate) (Cell Signaling Technology)] or PE-N-CAD [PE anti-human CD325 (N-cadherin) Antibody (Biolegend)] were added at concentrations of 1 µg/ml and 0.5 µg/ml, respectively. The tubes were incubated for 1 h, at room temperature. Flow cytometric analysis was carried out in the FACS Calibur flow cytometry system (Becton-Dickinson). Optimization of the antibodies was performed through antibody titrations in non-stimulated cells, using serial dilutions of E- and N-cadherin.

Retrieval of proteomic datasets and quantitative investigations

Secretome analysis of 13 CRC cell lines (HT29, SW480, SW620, HCT116, LoVo, RKO, LS180, LS174T, Colo320HSR, Colo205, DLD1, WiDr and SW1116) was previously described (Karagiannis et al., 2014b). Secretome analysis of cocultures between SW480/SW620 colon cancer cell lines with normal colonic fibroblasts 18Co was previously described (Karagiannis et al., 2012a). These proteomic datasets were retrieved from supplemental material of these studies, and a previous method (Collier et al., 2011) was used to normalize total spectral counts.

In silico investigations

Gene-expression meta-analysis Gene-expression meta-analysis was performed with Genevestigator (https://www.genevestigator.com), a web tool compiled with data from public repositories. The default platform Human133_2 (i.e., Human Genome 47k Array) was selected. Lists with official gene names were used as input, and all available probes mapped back to these gene IDs were selected for further analysis. The *perturbations* tool was used to investigate relative expression of specific gene probes between colon cancer and normal tissues. Fold-differences from multiple probes of the same gene were all combined in one score, and these were subsequently averaged from multiple studies to create one mean x-fold difference per gene. Representative heat maps were exported for visualization purposes.

Gene expression-based survival analysis Survival analysis was performed using PROGgene (http://www.compbio.iupui.edu/proggene), a web tool compiled with data from public repositories, such as GEO, EBI Array Express and The Cancer Genome Atlas, encompassing 64 patient series from 18 cancer types (Goswami and Nakshatri, 2013). In the process of performing survival analysis and creating prognostic plots, the web-based tool uses median gene-expression value to divide samples into 'High' and 'Low' gene expression groups, and subsequently uses survival data to create Cox proportional hazards models, by including hazard ratios and long rank *p*-values (Goswami and Nakshatri, 2013). The meta-analysis comprised of a total of two studies (Smith et al., 2009; Loboda et al., 2011) (Loboda, GSE28814; Smith, GSE17536 and GSE17537), which included microarray data from 326 (Loboda), 55 (Smith; training dataset) and 177 (Smith; validation dataset) patients.

Immunohistochemical investigations

Retrieval of immunohistochemical cases Evaluation of protein expression and localization was performed in 30 archived cases of invasive CRC, for the following proteins/markers: β-catenin (β-CAT), occludin (OCLN), platelet/endothelial cell adhesion molecule (PECAM/CD31), α-smooth muscle actin (α-SMA), h-caldesmon (h-CALD), laminin-α3 (LAMA3), laminin-β1 (LAMB1), ki-67 antigen (Ki-67) and gremlin-1 (GREM1). For more information on the patient cohort, the staining process, the antibodies used, as well as the evaluation and scoring system, along with the negative and positive controls used in each case, please refer to our previous publications (Karagiannis et al., 2014a,c).

Comparison of GREM1 expression between normal and desmoplastic stromata We identified certain areas of the colonic mucosa bearing healthy colonic crypts, along with their pericryptal and submucosal stromata, all juxtaposed close to neoplastic lesions. These stromata were further evaluated as healthy/normal, after confirming negative immunoreactivity for α-SMA/h-CALD/LAMB1, to exclude the possibility of a reactive, cancer-associated stroma (i.e., CAFs). For each normal stroma selected in this way, the most proximal cancer invasion front was also identified for comparative purposes, and in this case, its respective peritumoral stroma was confirmed as desmoplastic, through strong immunoreactivity for α-SMA/LAMB1, and parallel negative immunoreactivity for h-CALD. A total of 42 stromata, half of which were considered as 'normal stromata' (n=21), while the other half as 'pathologic/desmoplastic stromata' (n=21), were finally incorporated in this study, and were evaluated for GREM1 expression.

Categorization of immunohistochemical areas according to their EMT status Specific inquiries were performed to link the topographical juxtaposition of GREM1 with contextual dedifferentiation (i.e., EMT-related phenomena) in desmoplastic interfaces. The areas selected in each case were subdivided into 'EMT-pertaining' and 'EMT-quiescent' to demonstrate an active or non-active dedifferentiation process, respectively. Criteria for designating the areas as 'EMT-pertaining' were the following two prominent hallmarks of EMT (Kalluri and Weinberg, 2009): (I) cancer cells positioned at the periphery of the cohorts presented with nuclear accumulation of β-CAT, while those in the core of the cohorts with membranous, and (II) the expression levels of occludin (OCLN) may or may not present with

similar gradation; however, a progressive loss in the expression of OCLN in these cancer cells, when compared to control areas (i.e., normal colonic mucosa) and earlier invasion areas should be present. A failure to fulfill either of these two criteria categorized the areas as 'EMT-quiescent'. Representative figures, which clearly portray the differences between cells expressing nuclear β-CAT translocation, as well as the OCLN gradation, are shown in Figure S2.

Investigation of GREM1 expression in submucosal invasion fronts (SIFs) Areas of early cancer invasion, here termed as 'submucosal invasion fronts', with the typical appearance of cancer cell cohorts penetrating the submucosa after completely invading the muscularis mucosae, were selected. These areas were identified using a combination of β-catenin, LAMA3 and OCLN to spot the epithelial cancer cell cohorts, and α-SMA/h-CALD and LAMB1 to clearly demarcate the presence of peritumoral desmoplastic lesions in the parallel absence of smooth muscle cells belonging to the muscularis externa. A total of 110 SIFs were found in these 30 archived cases, for which co-assessment of β-CAT localization and OCLN gradation successfully categorized them into 58 'EMT-pertaining' and 52 'EMT-quiescent' areas.

Investigation of GREM1 expression in tumor nests (TNs) Submucosal areas of isolated, cancer cell aggregates with absence of glandular or pseudoglandular architecture, also known as TNs, were selected. Such aggregates might have possibly detached from a larger cancer cell cohort/collective invading the stroma through a poorly understood mechanism of pathogenesis (Weiss and Ward, 1983). The most attractive speculation is that of a stiffness-mediated disconnection through intense mechanical and reciprocal interactions of cancer collectives with the tumor-associated stroma (Werfel et al., 2013). The fate of these smaller TNs is currently unknown, despite preliminary evidence has been linking them with a passive, invasion-independent metastatic pathway, initiated by intravasation of tumor nests enveloped by endothelial cells of sinusoidal vasculature (Sugino et al., 2002, 2004; Kukko et al., 2010). A total of 42 TNs were identified in these archived cases, and they were further subdivided into 31 'EMT-pertaining' and 11 'EMT-quiescent' areas, using the co-assessment of β-CAT translocation and OCLN gradation.

Investigation of GREM1 expression in intramuscular invasion fronts (IIFs) Areas of deep cancer invasion, here termed as 'intramuscular invasion fronts', which present with the typical appearance of finger-like projections penetrating the smooth muscle layer (i.e., muscularis externa) were selected. These areas were identified using a combination of β-catenin, LAMA3 and OCLN to spot the epithelial cancer cell cohorts, and α-SMA/h-CALD to clearly demarcate the muscularis externa. A total of 28 IIF areas were found in these archived cases, for which the co-assessment of β-CAT translocation and OCLN gradation successfully categorized them into 21 'EMT-pertaining' and seven 'EMT-quiescent' areas.

Investigation of GREM1 expression in hypo- and hypervascular invasion fronts (HIFs) Vascular density was assessed by computer-assisted measurement of pixels in CD31-positive areas, as elsewhere described (Rooijens et al., 2004). Four to eight areas, encompassing a total of 168, were selected from the archived cases in an unbiased manner (i.e., through β-CAT). These invasion fronts were then mapped to their respective CD31 stains, and pictures were taken in low power field (×40) to assess vascular density. These pictures were uploaded into ImageJ software, where the CD31-positive area was measured in each case independently. The 168 areas were ranked from lower to higher, and subdivided into hypovascular (CD31-low; n=84) and hypervascular (CD31-high; n=84) invasion fronts (HIFs), with the median serving as cut-off.

Statistical analysis

Statistical analysis was performed in SPSS (version 20). Statistical differences were assessed with the following non-parametric tests: (a) Jonckheere-Terpstra test for multiple independent groups, (b) Mann-Whitney *U*-test for two independent groups, and (c) Wilcoxon test for two matched (paired) groups. All aforementioned data were shown as means with standard errors. Correlations were tested with the Spearman's ranked correlation coefficient. These data were presented as scatter plots with *p*-values and coefficient of determination (r^2). Statistical significance was shown at the 0.05 level, and whenever necessary, *p*-values were adjusted for multiple-hypothesis testing, using Holms-correction.

Competing Interests: The authors declare no financial and non-financial competing interests

Acknowledgments: George S Karagiannis is supported by the University Health Network and Mount Sinai Hospital, Toronto, Ontario, Canada. The authors would like to thank Chris Smith, Ihor Batruch, Annie Bang, Kuruzar Gordana and Antoninus Soosapillai for technical assistance.

References

Ahmed, D., Eide, P.W., Eilertsen, I.A., Danielsen, S.A., Eknaes, M., Hektoen, M., Lind, G.E., and Lothe, R.A. (2013). Epigenetic and genetic features of 24 colon cancer cell lines. Oncogenesis *2*, e71.

Akcakaya, H., Aroymak, A., and Gokce, S. (2007). A. quantitative colorimetric method of measuring alkaline phosphatase activity in eukaryotic cell membranes. Cell. Biol. Int. *31*, 186–190.

Alison, M.R., Lin, W.R., Lim, S.M., and Nicholson, L.J. (2012). Cancer stem cells: in the line of fire. Cancer Treat. Rev. *38*, 589–598.

Bates, R.C. and Mercurio, A.M. (2005). The epithelial-mesenchymal transition (EMT) and colorectal cancer progression. Cancer Biol. Ther. *4*, 365–370.

Beck, S.E., Jung, B.H., Fiorino, A., Gomez, J., Rosario, E.D., Cabrera, B.L., Huang, S.C., Chow, J.Y., and Carethers, J.M. (2006). Bone morphogenetic protein signaling and growth suppression in colon cancer. Am. J. Physiol. Gastrointest. Liver Physiol. *291*, G135–G145.

Beck, S.E., Jung, B.H., Del Rosario, E., Gomez, J., and Carethers, J.M. (2007). BMP-induced growth suppression in colon cancer cells is mediated by p21WAF1 stabilization and modulated by RAS/ERK. Cell Signal. *19*, 1465–1472.

Beites, C.L., Hollenbeck, P.L., Kim, J., Lovell-Badge, R., Lander, A.D., and Calof, A.L. (2009). Follistatin modulates a BMP autoregulatory loop to control the size and patterning of sensory domains in the developing tongue. Development *136*, 2187–2197.

Bendtsen, J.D., Jensen, L.J., Blom, N., Von Heijne, G., and Brunak, S. (2004). Feature-based prediction of non-classical and leaderless protein secretion. Protein Eng. Des. Sel. *17*, 349–356.

Beppu, H., Mwizerwa, O.N., Beppu, Y., Dattwyler, M.P., Lauwers, G.Y., Bloch, K.D., and Goldstein, A.M. (2008). Stromal inactivation of BMPRII leads to colorectal epithelial overgrowth and polyp formation. Oncogene *27*, 1063–1070.

Bertrand, F.E., Angus, C.W., Partis, W.J., and Sigounas, G. (2012). Developmental pathways in colon cancer: crosstalk between WNT, BMP, Hedgehog and Notch. Cell Cycle *11*, 4344–4351.

Bhowmick, N.A. and Moses, H.L. (2005). Tumor-stroma interactions. Curr. Opin. Genet. Dev. *15*, 97–101.

Bissell, M.J. and Radisky, D. (2001). Putting tumours in context. Nat. Rev. Cancer *1*, 46–54.

Boland, C.R. and Goel, A. (2010). Microsatellite instability in colorectal cancer. Gastroenterology *138*, 2073–2087 e3.

Brabletz, T., Jung, A., Spaderna, S., Hlubek, F., and Kirchner, T. (2005). Opinion: migrating cancer stem cells – an integrated concept of malignant tumour progression. Nat. Rev. Cancer *5*, 744–749.

Cai, Z.G., Zhang, S.M., Zhang, H., Zhou, Y.Y., Wu, H.B., and Xu, X.P. (2013). Aberrant expression of microRNAs involved in epithelial-mesenchymal transition of HT-29 cell line. Cell. Biol. Int. *37*, 669–674.

Chen, D., Zhao, M., and Mundy, G.R. (2004). Bone morphogenetic proteins. Growth Factors *22*, 233–241.

Chen, M.H., Yeh, Y.C., Shyr, Y.M., Jan, Y.H., Chao, Y., Li, C.P., Wang, S.E., Tzeng, C.H., Chang, P.M., Liu, C.Y., et al. (2012). Expression of gremlin 1 correlates with increased angiogenesis and progression-free survival in patients with pancreatic neuroendocrine tumors. J. Gastroenterol. *48*, 101–108.

Collier, T.S., Randall, S.M., Sarkar, P., Rao, B.M., Dean, R.A., and Muddiman, D.C. (2011). Comparison of stable-isotope labeling with amino acids in cell culture and spectral counting for relative quantification of protein expression. Rapid Commun. Mass Spectrom. *25*, 2524–2532.

De Wever, O., Pauwels, P., De Craene, B., Sabbah, M., Emami, S., Redeuilh, G., Gespach, C., Bracke, M., and Berx, G. (2008). Molecular and pathological signatures of epithelial-mesenchymal transitions at the cancer invasion front. Histochem. Cell Biol. *130*, 481–494.

Deng, H., Makizumi, R., Ravikumar, T.S., Dong, H., Yang, W., and Yang, W.L. (2007a). Bone morphogenetic protein-4 is overexpressed in colonic adenocarcinomas and promotes migration and invasion of HCT116 cells. Exp. Cell Res. *313*, 1033–1044.

Deng, H., Ravikumar, T.S., and Yang, W.L. (2007b). Bone morphogenetic protein-4 inhibits heat-induced apoptosis by modulating MAPK pathways in human colon cancer HCT116 cells. Cancer Lett. *256*, 207–217.

Deng, H., Ravikumar, T.S., and Yang, W.L. (2009). Overexpression of bone morphogenetic protein 4 enhances the invasiveness of Smad4-deficient human colorectal cancer cells. Cancer Lett. *281*, 220–231.

Elenbaas, B. and Weinberg, R.A. (2001). Heterotypic signaling between epithelial tumor cells and fibroblasts in carcinoma formation. Exp. Cell Res. *264*, 169–184.

Gazzerro, E. and Canalis, E. (2006). Bone morphogenetic proteins and their antagonists. Rev. Endocr. Metab. Disord. *7*, 51–65.

Goswami, C.P. and Nakshatri, H. (2013). PROGgene: gene expression based survival analysis web application for multiple cancers. J. Clin. Bioinforma *3*, 22.

Grijelmo, C., Rodrigue, C., Svrcek, M., Bruyneel, E., Hendrix, A., de Wever, O., and Gespach, C. (2007). Proinvasive activity of BMP-7 through SMAD4/src-independent and ERK/Rac/JNK-dependent signaling pathways in colon cancer cells. Cell Signal. *19*, 1722–1732.

Hanahan, D. and Weinberg, R.A. (2011). Hallmarks of cancer: the next generation. Cell *144*, 646–674.

Hardwick, J.C., Van Den Brink, G.R., Bleuming, S.A., Ballester, I., Van Den Brande, J.M., Keller, J.J., Offerhaus, G.J., Van Deventer, S.J., and Peppelenbosch, M.P. (2004). Bone morphogenetic protein 2 is expressed by, and acts upon, mature epithelial cells in the colon. Gastroenterology *126*, 111–121.

Hardwick, J.C., Kodach, L.L., Offerhaus, G.J., and van den Brink, G.R. (2008). Bone morphogenetic protein signalling in colorectal cancer. Nat. Rev. Cancer *8*, 806–812.

He, X.C., Zhang, J., Tong, W.G., Tawfik, O., Ross, J., Scoville, D.H., Tian, Q., Zeng, X., He, X., Wiedemann, L.M., et al. (2004). BMP signaling inhibits intestinal stem cell self-renewal through suppression of Wnt-β-catenin signaling. Nat. Genet. *36*, 1117–1121.

Hirakawa, M., Takimoto, R., Tamura, F., Yoshida, M., Ono, M., Murase, K., Sato, Y., Osuga, T., Sato, T., Iyama, S., et al. (2013). Fucosylated TGF-beta receptors transduces a signal for epithelial-mesenchymal transition in colorectal cancer cells. Br. J. Cancer *110*, 156–163.

Ilyas, M., Straub, J., Tomlinson, I.P., and Bodmer, W.F. (1999). Genetic pathways in colorectal and other cancers. Eur. J. Cancer *35*, 335–351.

Ishizuya-Oka, A. (2005). Epithelial-connective tissue cross-talk is essential for regeneration of intestinal epithelium. J. Nippon Med. Sch. *72*, 13–18.

Jain, K.K. (2008). Innovations, challenges and future prospects of oncoproteomics. Mol. Oncol. *2*, 153–160.

Kalluri, R. (2009). EMT: when epithelial cells decide to become mesenchymal-like cells. J. Clin. Invest. *119*, 1417–1419.

Kalluri, R. and Weinberg, R.A. (2009). The basics of epithelial-mesenchymal transition. J. Clin. Invest. *119*, 1420–1428.

Kang, M.H., Kang, H.N., Kim, J.L., Kim, J.S., Oh, S.C., and Yoo, Y.A. (2009). Inhibition of PI3 kinase/Akt pathway is required for BMP2-induced EMT and invasion. Oncol. Rep. *22*, 525–534.

Karagiannis, G.S., Pavlou, M.P., and Diamandis, E.P. (2010). Cancer secretomics reveal pathophysiological pathways in cancer molecular oncology. Mol. Oncol. *4*, 496–510.

Karagiannis, G.S., Petraki, C., Prassas, I., Saraon, P., Musrap, N., Dimitromanolakis, A., and Diamandis, E.P. (2012a). Proteomic signatures of the desmoplastic invasion front reveal collagen type XII as a marker of myofibroblastic differentiation during colorectal cancer metastasis. Oncotarget *3*, 267–285.

Karagiannis, G.S., Poutahidis, T., Erdman, S.E., Kirsch, R., Riddell, R.H., and Diamandis, E.P. (2012b). Cancer-associated fibroblasts drive the progression of metastasis through both paracrine and mechanical pressure on cancer tissue. Mol. Cancer Res. *10*, 1403–1418.

Karagiannis, G.S., Berk, A., Dimitromanolakis, A., and Diamandis, E.P. (2013). Enrichment map profiling of the cancer invasion front suggests regulation of colorectal cancer progression by

the bone morphogenetic protein antagonist, gremlin-1. Mol. Oncol. *7*, 826–839.

Karagiannis, G.S., Schaeffer, D.F., Cho, C.K., Musrap, N., Saraon, P., Batruch, I., Grin, A., Mitrovic, B., Kirsch, R., Riddell, R.H., et al. (2014a). Collective migration of cancer-associated fibroblasts is enhanced by overexpression of tight junction-associated proteins claudin-11 and occludin. Mol. Oncol. *8*, 178–195.

Karagiannis, G.S., Pavlou, M.P., Saraon, P., Musrap, N., Xie, A., Batruch, I., Prassas, I., Dimitromanolakis, A., Petraki, C., and Diamandis, E.P. (2014b). In-depth proteomic delineation of the colorectal cancer exoproteome: Mechanistic insight and identification of potential biomarkers. J. Proteomics *103*, 121–136.

Karagiannis, G.S., Treacy, A., Messenger, D., Grin, A., Kirsch, R., Riddell, R.H., and Diamandis, E,P. (2014c) Expression patterns of bone morphogenetic protein antagonists in colorectal cancer desmoplastic invasion fronts. Mol. Oncol., in press.

Khokha, M.K., Hsu, D., Brunet, L.J., Dionne, M.S., and Harland, R.M. (2003). Gremlin is the BMP antagonist required for maintenance of Shh and Fgf signals during limb patterning. Nat. Genet. *34*, 303–307.

Kishigami, S. and Mishina, Y. (2005). BMP signaling and early embryonic patterning. Cytokine Growth Factor Rev. *16*, 265–278.

Kodach, L.L., Bleuming, S.A., Musler, A.R., Peppelenbosch, M.P., Hommes, D.W., van den Brink, G.R., van Noesel, C.J., Offerhaus, G.J., and Hardwick, J.C. (2008). The bone morphogenetic protein pathway is active in human colon adenomas and inactivated in colorectal cancer. Cancer *112*, 300–306.

Kosinski, C., Li, V.S., Chan, A.S., Zhang, J., Ho, C., Tsui, W.Y., Chan, T.L., Mifflin, R.C., Powell, D.W., Yuen, S.T., et al. (2007). Gene expression patterns of human colon tops and basal crypts and BMP antagonists as intestinal stem cell niche factors. Proc. Natl. Acad. Sci. USA *104*, 15418–15423.

Kukko, H.M., Koljonen, V.S., Tukiainen, E.J., Haglund, C.H., and Bohling, T.O. (2010). Vascular invasion is an early event in pathogenesis of Merkel cell carcinoma. Mod. Pathol. *23*, 1151–1156.

Kulasingam, V. and Diamandis, E.P. (2008). Tissue culture-based breast cancer biomarker discovery platform. Int. J. Cancer *123*, 2007–2012.

Kunz-Schughart, L.A. and Knuechel, R. (2002a). Tumor-associated fibroblasts (part I): Active stromal participants in tumor development and progression? Histol. Histopathol. *17*, 599–621.

Kunz-Schughart, L.A. and Knuechel, R. (2002b). Tumor-associated fibroblasts (part II): Functional impact on tumor tissue. Histol. Histopathol. *17*, 623–637.

Lappin, D.W., McMahon, R., Murphy, M., and Brady, H.R. (2002). Gremlin: an example of the re-emergence of developmental programmes in diabetic nephropathy. Nephrol. Dial. Transplant *17* (Suppl *9*), 65–67.

Li, Y., Zhu, X., Zeng, Y., Wang, J., Zhang, X., Ding, Y.Q., and Liang, L. (2010). FMNL2 enhances invasion of colorectal carcinoma by inducing epithelial-mesenchymal transition. Mol. Cancer Res. *8*, 1579–1590.

Loboda, A., Nebozhyn, M.V., Watters, J.W., Buser, C.A., Shaw, P.M., Huang, P.S., Van't Veer, L., Tollenaar, R.A., Jackson, D.B., Agrawal, D., et al. (2011). EMT is the dominant program in human colon cancer. BMC Med. Genomics *4*, 9.

Lorente-Trigos, A., Varnat, F., Melotti, A., and Ruiz i Altaba, A. (2010). BMP signaling promotes the growth of primary human colon carcinomas *in vivo*. J. Mol. Cell. Biol. *2*, 318–332.

Markowitz, S.D. and Bertagnolli, M.M. (2009). Molecular origins of cancer: Molecular basis of colorectal cancer. N. Engl. J. Med. *361*, 2449–2460.

Mezzano, S., Droguett, A., Burgos, M.E., Aros, C., Ardiles, L., Flores, C., Carpio, D., Carvajal, G., Ruiz-Ortega, M., and Egido, J. (2007). Expression of gremlin, a bone morphogenetic protein antagonist, in glomerular crescents of pauci-immune glomerulonephritis. Nephrol. Dial. Transplant. *22*, 1882–1890.

Michos, O., Panman, L., Vintersten, K., Beier, K., Zeller, R., and Zuniga, A. (2004). Gremlin-mediated BMP antagonism induces the epithelial-mesenchymal feedback signaling controlling metanephric kidney and limb organogenesis. Development *131*, 3401–3410.

Michos, O., Goncalves, A., Lopez-Rios, J., Tiecke, E., Naillat, F., Beier, K., Galli, A., Vainio, S., and Zeller, R. (2007). Reduction of BMP4 activity by gremlin 1 enables ureteric bud outgrowth and GDNF/WNT11 feedback signalling during kidney branching morphogenesis. Development *134*, 2397–2405.

Mitola, S., Ravelli, C., Moroni, E., Salvi, V., Leali, D., Ballmer-Hofer, K., Zammataro, L., and Presta, M. (2010). Gremlin is a novel agonist of the major proangiogenic receptor VEGFR2. Blood *116*, 3677–3680.

Mitrovic, B., Schaeffer, D.F., Riddell, R.H., and Kirsch, R. (2012). Tumor budding in colorectal carcinoma: time to take notice. Mod. Pathol. *25*, 1315–1325.

Miyazono, K., Maeda, S., and Imamura, T. (2005). BMP receptor signaling: transcriptional targets, regulation of signals, and signaling cross-talk. Cytokine Growth Factor Rev. *16*, 251–263.

Motoyama, K., Tanaka, F., Kosaka, Y., Mimori, K., Uetake, H., Inoue, H., Sugihara, K., and Mori, M. (2008). Clinical significance of BMP7 in human colorectal cancer. Ann. Surg. Oncol. *15*, 1530–1537.

Mulvihill, M.S., Kwon, Y.W., Lee, S., Fang, L.T., Choi, H., Ray, R., Kang, H.C., Mao, J.H., Jablons, D., and Kim, I.J. (2012). Gremlin is overexpressed in lung adenocarcinoma and increases cell growth and proliferation in normal lung cells. PLoS One *7*, e42264.

Murphy, M., McMahon, R., Lappin, D.W., and Brady, H.R. (2002). Gremlins: is this what renal fibrogenesis has come to? Exp. Nephrol. *10*, 241–244.

Myllärniemi, M., Lindholm, P., Ryynanen, M.J., Kliment, C.R., Salmenkivi, K., Keski-Oja, J., Kinnula, V.L., Oury, T.D., and Koli, K. (2008). Gremlin-mediated decrease in bone morphogenetic protein signaling promotes pulmonary fibrosis. Am. J. Respir. Crit. Care Med. *177*, 321–329.

Navab, R., Strumpf, D., Bandarchi, B., Zhu, C.Q., Pintilie, M., Ramnarine, V.R., Ibrahimov, E., Radulovich, N., Leung, L., Barczyk, M., et al. (2011). Prognostic gene-expression signature of carcinoma-associated fibroblasts in non-small cell lung cancer. Proc. Natl. Acad. Sci. USA *108*, 7160–7165.

Nishanian, T.G., Kim, J.S., Foxworth, A., and Waldman, T. (2004). Suppression of tumorigenesis and activation of Wnt signaling by bone morphogenetic protein 4 in human cancer cells. Cancer Biol. Ther. *3*, 667–675.

Orimo, A., Gupta, P.B., Sgroi, D.C., Arenzana-Seisdedos, F., Delaunay, T., Naeem, R., Carey, V.J., Richardson, A.L., and Weinberg, R.A. (2005). Stromal fibroblasts present in invasive human breast carcinomas promote tumor growth and angiogenesis through elevated SDF-1/CXCL12 secretion. Cell *121*, 335–348.

Owens, P., Pickup, M.W., Novitskiy, S.V., Chytil, A., Gorska, A.E., Aakre, M.E., West, J., and Moses, H.L. (2011) Disruption of bone morphogenetic protein receptor 2 (BMPR2) in mammary tumors promotes metastases through cell autonomous and paracrine mediators. Proc. Natl. Acad. Sci. USA *109*, 2814–2819.

Owens, P., Polikowsky, H., Pickup, M.W., Gorska, A.E., Jovanovic, B., Shaw, A.K., Novitskiy, S.V., Hong, C.C., and Moses, H.L. (2013). Bone Morphogenetic Proteins stimulate mammary fibroblasts to promote mammary carcinoma cell invasion. PLoS One *8*, e67533.

Ravelli, C., Mitola, S., Corsini, M., and Presta, M. (2012). Involvement of alphavbeta3 integrin in gremlin-induced angiogenesis. Angiogenesis *16*, 235–243.

Rooijens, P.P., de Krijger, R.R., Bonjer, H.J., van der Ham, F., Nigg, A.L., Bruining, H.A., Lamberts, S.W., and van der Harst, E. (2004). The significance of angiogenesis in malignant pheochromocytomas. Endocr. Pathol. *15*, 39–45.

Roxburgh, S.A., Kattla, J.J., Curran, S.P., O'Meara, Y.M., Pollock, C.A., Goldschmeding, R., Godson, C., Martin, F., and Brazil, D.P. (2009). Allelic depletion of grem1 attenuates diabetic kidney disease. Diabetes *58*, 1641–1650.

Sääf, A.M., Halbleib, J.M., Chen, X., Yuen, S.T., Leung, S.Y., Nelson, W.J., and Brown, P.O. (2007). Parallels between global transcriptional programs of polarizing Caco-2 intestinal epithelial cells in vitro and gene expression programs in normal colon and colon cancer. Mol. Biol. Cell *18*, 4245–4260.

Saraon, P., Musrap, N., Cretu, D., Karagiannis, G.S., Batruch, I., Smith, C., Drabovich, A.P., Trudel, D., van der Kwast, T., Morrissey, C., et al. (2012). Proteomic profiling of androgen-independent prostate cancer cell lines reveals a role for protein, S. during the development of high grade and castration-resistant prostate cancer. J. Biol. Chem. *287*, 34019–34031.

Saraon, P., Cretu, D., Musrap, N., Karagiannis, G.S., Batruch, I., Drabovich, A.P., van der Kwast, T., Mizokami, A., Morrissey, C., Jarvi, K., et al. (2013). Quantitative proteomics reveals that enzymes of the ketogenic pathway are associated with prostate cancer progression. Mol. Cell Proteomics *12*, 1589–1601.

Scheel, C. and Weinberg, R.A. (2012). Cancer stem cells and epithelial-mesenchymal transition: concepts and molecular links. Semin. Cancer Biol. *22*, 396–403.

Sell, S. (2010). On the stem cell origin of cancer. Am. J. Pathol *176*, 2584–494.

Shen, L., Qu, X., Ma, Y., Zheng, J., Chu, D., Liu, B., Li, X., Wang, M., Xu, C., Liu, N., et al. (2014). Tumor suppressor NDRG2 tips the balance of oncogenic TGF-beta via EMT inhibition in colorectal cancer. Oncogenesis *3*, e86.

Slattery, M.L., Lundgreen, A., Herrick, J.S., Kadlubar, S., Caan, B.J., Potter, J.D., and Wolff, R.K. (2011a). Genetic variation in bone morphogenetic protein and colon and rectal cancer. Int. J. Cancer *130*, 653–664.

Slattery, M.L., Lundgreen, A., Herrick, J.S., Wolff, R.K., and Caan, B.J. (2011b). Genetic variation in the transforming growth factor-beta signaling pathway and survival after diagnosis with colon and rectal cancer. Cancer *117*, 4175–4183.

Smith, J.J., Deane, N.G., Wu, F., Merchant, N.B., Zhang, B., Jiang, A., Lu, P., Johnson, J.C., Schmidt, C., Bailey, C.E., et al. (2009). Experimentally derived metastasis gene expression profile predicts recurrence and death in patients with colon cancer. Gastroenterology *138*, 958–968.

Sneddon, J.B. (2009). The contribution of niche-derived factors to the regulation of cancer cells. Methods Mol. Biol. *568*, 217–232.

Sneddon, J.B. and Werb, Z. (2007). Location, location, location: the cancer stem cell niche. Cell Stem Cell *1*, 607–611.

Sneddon, J.B., Zhen, H.H., Montgomery, K., van de Rijn, M., Tward, A.D., West, R., Gladstone, H., Chang, H.Y., Morganroth, G.S., Oro, A.E., et al. (2006). Bone morphogenetic protein antagonist gremlin 1 is widely expressed by cancer-associated stromal cells and can promote tumor cell proliferation. Proc. Natl. Acad. Sci. USA *103*, 14842–14847.

Souvannavong, V., Lemaire, C., De Nay, D., Brown, S., and Adam, A. (1995). Expression of alkaline phosphatase by a B-cell hybridoma and its modulation during cell growth and apoptosis. Immunol. Lett. *47*, 163–170.

Spaderna, S., Schmalhofer, O., Hlubek, F., Jung, A., Kirchner, T., and Brabletz, T. (2007). Epithelial-mesenchymal and mesenchymal-epithelial transitions during cancer progression. Verh. Dtsch. Ges. Pathol. *91*, 21–28.

Stabile, H., Mitola, S., Moroni, E., Belleri, M., Nicoli, S., Coltrini, D., Peri, F., Pessi, A., Orsatti, L., Talamo, F., et al. (2007). Bone morphogenic protein antagonist Drm/gremlin is a novel proangiogenic factor. Blood *109*, 1834–1840.

Sugino, T., Kusakabe, T., Hoshi, N., Yamaguchi, T., Kawaguchi, T., Goodison, S., Sekimata, M., Homma, Y., and Suzuki, T. (2002). An invasion-independent pathway of blood-borne metastasis: a new murine mammary tumor model. Am. J. Pathol. *160*, 1973–1980.

Sugino, T., Yamaguchi, T., Ogura, G., Saito, A., Hashimoto, T., Hoshi, N., Yoshida, S., Goodison, S., and Suzuki, T. (2004). Morphological evidence for an invasion-independent metastasis pathway exists in multiple human cancers. BMC Med. *2*, 9.

Tse, J.C. and Kalluri, R. (2007). Mechanisms of metastasis: epithelial-to-mesenchymal transition and contribution of tumor microenvironment. J. Cell. Biochem. *101*, 816–829.

von Bubnoff, A. and Cho, K.W. (2001). Intracellular BMP signaling regulation in vertebrates: pathway or network? Dev. Biol. *239*, 1–14.

von Kleist, S., Chany, E., Burtin, P., King, M., and Fogh, J. (1975). Immunohistology of the antigenic pattern of a continuous cell line from a human colon tumor. J. Natl. Cancer Inst. *55*, 555–560.

Watnick, R.S. (2012). The role of the tumor microenvironment in regulating angiogenesis. Cold Spring Harb. Perspect. Med. *2*, a006676.

Weiss, L. and Ward, P.M. (1983). Cell detachment and metastasis. Cancer Metastasis Rev. *2*, 111–127.

Werfel, J., Krause, S., Bischof, A.G., Mannix, R.J., Tobin, H., Bar-Yam, Y., Bellin, R.M., and Ingber, D.E. (2013). How changes in extracellular matrix mechanics and gene expression variability might combine to drive cancer progression. PLoS One *8*, e76122.

Wu, W.K., Sung, J.J., Wu, Y.C., Li, Z.J., Yu, L., and Cho, C.H. (2008). Bone morphogenetic protein signalling is required for the anti-mitogenic effect of the proteasome inhibitor MG-132 on colon cancer cells. Br. J. Pharmacol. *154*, 632–638.

Xu, R.H., Peck, R.M., Li, D.S., Feng, X., Ludwig, T., and Thomson, J.A. (2005). Basic FGF and suppression of BMP signaling sustain undifferentiated proliferation of human, E.S. cells. Nat. Methods *2*, 185–190.

Yan, K., Wu, Q., Yan, D.H., Lee, C.H., Rahim, N., Tritschler, I., DeVecchio, J., Kalady, M.F., Hjelmeland, A.B., Rich, J.N. (2014). Glioma cancer stem cells secrete Gremlin1 to promote their maintenance within the tumor hierarchy. Genes Dev. *28*, 1085–1100.

Zeisberg, E.M., Potenta, S., Xie, L., Zeisberg, M., and Kalluri, R. (2007). Discovery of endothelial to mesenchymal transition as a source for carcinoma-associated fibroblasts. Cancer Res. *67*, 10123–10128.

Zhang, J.F., Fu, W.M., He, M.L., Xie, W.D., Lv, Q., Wan, G., Li, G., Wang, H., Lu, G., Hu, X., et al. (2011). MiRNA-20a promotes osteogenic differentiation of human mesenchymal stem cells by co-regulating BMP signaling. RNA Biol. *8*, 829–838.

Zlobec, I. and Lugli, A. (2011). Epithelial mesenchymal transition and tumor budding in aggressive colorectal cancer: tumor budding as oncotarget. Oncotarget *1*, 651–661.

Supplemental Material: The online version of this article (DOI: 10.1515/hsz-2014-0221) offers supplementary material, available to authorized users.